UNIVERSIDAD DE CHILE
FACULTAD DE CIENCIAS FÍSICAS Y MATEMÁTICAS
DEPARTAMENTO DE INGENIERÍA MECÁNICA

ENERGY BALANCE IN GAS METAL ARC WELDING

MEMORIA PARA OPTAR AL TÍTULO DE INGENIERO CIVIL MECÁNICO

VICENTE ANDRÉS NÚÑEZ SÁNCHEZ

PROFESOR GUÍA:
PATRICIO MENDEZ PINTO

MIEMBROS DE LA COMISIÓN:
RUBÉN FERNANDEZ URRUTIA
ALI AKBARI-FAKHRABADI

SANTIAGO DE CHILE
2021

RESUMEN DE LA MEMORIA PARA OPTAR
AL TÍTULO DE INGENIERO CIVIL
MECÁNICO
POR: **VICENTE ANDRÉS NÚÑEZ SÁNCHEZ**
FECHA: 2021
PROF. GUÍA: PATRICIO MENDEZ PINTO

ENERGY BALANCE IN GAS METAL ARC WELDING

La soldadura es un método de unión de materiales que sobre metales es bastante usado en la industria. Es interesante notar que los que más entienden son los operarios, quienes regulan los parámetros iniciales. Para los distintos procesos manuales, resulta bastante difícil poder encontrar un proceso óptimo sin conocer la física detrás del proceso. Este trabajo permite comprender la teoría presente en la gota generada para el proceso de Gas Metal Arc Welding (GMAW) y sus distintos efectos.

La soldadura GMAW presenta principalmente un gas protector y un electrodo positivo consumible, siendo el voltaje, la velocidad de avance del electrodo y la distancia entre el electrodo y el objeto a soldar las variables a controlar por el soldador. Estas son unas de las tantas variables existentes en la física detrás del arco generado. Una de estas variables es una potencia que se genera en el ánodo, la cual permitiría comprender mejor la temperatura de la gota generada.

El desarrollo de un balance energético en el electrodo es realizado para poder luego obtener de la potencia del ánodo, una caída de voltaje en este. Para obtener este último valor y comprender su comportamiento es necesario comprender de buena manera la masa que se evapora en la gota, por lo que se el desarrollo de un modelo se realizó. Evaporaciones menores al 10% fueron obtenidas en su mayoría, presentando voltajes menores a 6 V, con ciertas tendencias. Al considerar las distintas composiciones de los electrodos, se puede ver como varían con respecto a cada resultado. Estos resultados eran los que se esperaban obtener, como también sus tendencias.

Finalmente queda comentar las utilidades que el trabajo presente puede tener, como también ciertos lineamientos de futuros trabajos que puedan realizarse a partir de este. Las aplicaciones de la caída de voltaje puede realizarse para distintos cálculos de potencia. Los perfiles químicos de evaporación pueden ser también aplicados para otros modelos energéticos.

RESUMEN DE LA MEMORIA PARA OPTAR
AL TÍTULO DE INGENIERO CIVIL
MECÁNICO
POR: **VICENTE ANDRÉS NÚÑEZ SÁNCHEZ**
FECHA: 2021
PROF. GUÍA: PATRICIO MENDEZ PINTO

ENERGY BALANCE IN GAS METAL ARC WELDING

Welding as a joining method for materials is one of the most used in industry. It is interesting to notice that the people that most understand of the process are the operators, the ones that have to regulate the different parameters. As a manual process, it is difficult to find an optimum range of operation, without knowing all the physics behind the weld. This work allows to comprehend a small part of the theory behind the droplet that is deposited on the welding pool at the Gas Metal Arc Welding (GMAW) process.

The GMAW process presents a shielding gas and a positive electrode that is consumable, being the voltage, the wire feed speed (WFS) and the contact tip to work piece distance (CTWD) the variables to control by the welder. These are just ones of the various variables behind the physics of the arc that is generated. Over the droplet it is placed a power loss, that is studied as the anode fall voltage.

The development of an energy balance on the electrode is to obtain this anode fall voltage. To obtain the value and understand its behaviour, it is necessary to understand the mass that evaporates from the droplet, so a model is also generated. Evaporations lower than a 10% of the mass that enters the system was obtained with anode fall voltages lower than 6 V in many cases. When considering the composition of the electrode, the values changed considerably. This values were expected and also the different trends.

Finally the main point to analyse is the utility of this work, as also some points to consider for future works. This different voltages and chemical evaporation profiles can be applied to different models that would vary with the composition of an electrode.

O yo me engaño,
o ésta ha de ser la más famosa aventura.

Acknowledgement

En primer lugar quiero agradecer a mi familia. Ellos son los que me han apoyado todos los días en cualquiera que sea mi aventura, desde ir a estudiar al extranjero hasta esas conversaciones para no estudiar. Mi madre que me dió la vida y no deja de recordármelo, mi papá que me motiva a dar ese paso extra siempre y mi hermano que no deja de repetirme lo inteligente que soy. Mis tíos y primas que disfrutan cada uno de mis chistes en todas las juntas familiares de día domingo.

En segundo lugar a mis amigos, que me han acompañado en los buenos y malos momentos. Markus que desde siempre me sacó una risa, incluso cuando no debíamos reírnos. Víctor y Javiera que me han hecho despertar muchas veces, siempre listos para levantarme de donde sea que me encuentre. Fernando por hacerme trabajar hasta muy tarde, pero asumiendo que yo lo haría trabajar desde temprano. Agradecido por cada amigo que me hice en el camino y por los que perduran en los aventuras venidas y por venir.

Mis compañeros del equipo de voleibol, que siempre tuve claro que eran mi segunda familia. Cada uno de ellos que tuve la suerte de conocer dentro y fuera de la cancha, fue parte de distintos momentos de historia para el equipo de voleibol de la facultad. Momentos malos hubieron y estuvimos acompañados. Momentos buenos hubieron muchos más y fue cuando las buenas historias se escribieron con amistad y esfuerzo.

Al profesor Patricio, que siempre tuvo una disposición increíble a ayudar durante mi proceso de trabajo de título y a dar buenos consejos. Al gobierno de Canadá y a la Universidad de Alberta por financiar mi estadía en Canadá para el desarrollo de mi tesis.

Tabla of Contents

Index of Tables

Index of Ilustrations

Chapter 1

Introduction

Welding is a joining process, that has been widely used in all kinds of industry: from mining, sports, bridges and computers. This joining process as it can be on different materials, has also many different ways to be reached. It could be as a manual or an automatic process. When looking at the manual process, the majority of welding are generated through a plasma arc. This plasma arc occurs close to the speed of sound and at temperatures higher than the sun [1]. Welding involves multi physics problems, that have been studied, but it does not contain solutions to problems. This solutions have still not arrived, because as the welding has been built over experience in years. When a new problem arrives it is less expensive and faster to make another weld instead of building the entire theory out of the physics to solve the problem. This understanding of the physics and the engineering solutions is what this work is meant to do: a first solution to a small welding problem.

Gas Metal Arc Welding is a process where the electrode works as a filler metal and is deposited on the base metal to join the different parts. This welding technique is considered to be semi-automatic, because the filler metal is being deposited in a constant feed by the operator. This operator is responsible to select the voltage and the wire feed speed (WFS) of the process, to after do the weld. As the welder knows how to weld and not all the physics behind the process, it is very unlikely that an optimum can be reached. Due to all the unknown variables, it is unlikely to reach an optimum solution and is known to result in faulty welds when applied to knew materials, or when attempting to comply with new standards.

An example of a problem can be the use of a specific material but it generates important mass that evaporates, that could be breathe by the welder and cause more serious problems. Nowadays there is not enough understanding to solve this evaporation problem on the droplet, but the approach of this work is a step to understand the physics behind of the droplet generated on the GMAW process and its temperature.

1.1. Motivation

When studying the droplet of the GMAW process, it is important to notice all the different heats that are entering and leaving the system. To understand all the heats in the system, a voltage is considered to be on the anode and that can be decomposed as a voltage fall [2]. It could be wrong to say that an anode voltage is present without the cathode, but this is to make a relation between the current that is going through and the heat that is generated at the anode spot.

Fumes are generated in different places during the process, being the melted droplet the one to study in this report. To calculate the mass evaporated in the melted droplet on the anode, it is necessary to understand the reason of evaporation in the droplet and thermal diffusion is they key according to Y. Cressault and A. Gleizesthe [3]. All the physics behind this problem is being expressed in this work and a first solution to understand the droplet temperature is given with the anode fall voltage.

To verify the model, data acquired by a previous CCWJ student was used. The main values for the validation included the physical properties of the electrode, and the droplet temperature according to a current. The whole work was supported by the CCWJ laboratory and the ELAP scholarship program.

1.2. Objectives

The main objective of this work is to develop a relationship between the droplet temperature, the anode fall voltage and the current of gas metal arc welding. To achieve this, it is necessary to accomplish the next steps:

- Understand the GMAW process.
- Analyse through an energy balance the droplet and the stick out.
- Estimate the mass evaporated with a mass balance on the droplet.
- Analyse the behaviour of the model with the data obtained.
- Analyse the model according to previous studies.

1.3. Scope of work

The following aspects are to be considered on the GMAW model developed.

- Generate a model of anode fall voltage based on an energy balance.
- Generate an evaporation model for a spherical droplet and with argon as shielding gas.
- Work only for direct current measurements.
- Generate a model for different electrode composition.

1.4. Literature Review

The welding process has being understood in different ways and one of those is under segregating every drop of power as a fall voltage times current. This allows engineers to see the system as different resistances or as different sources of power loss independent or with some dependence from current. This way of looking at the problem is interesting, because it makes the problem tangible and allows engineers to simplify it.

A work that gives some alignments is done by McIntosh and Mendez [4]. In this work the fall voltage and droplet heat content was determined for a pulsed waveform GMAW process. From this article was determined that overall the cathode fall voltage was independent from current, but may be still influenced by the material composition and temperatures. Also the anode fall voltage was determined to be independent from the current but with slight variations with different waveforms.

The main work recently done is by Zhang *et al.* [5] can be complemented by [6], gives values of what the anode fall voltage should be at a specific process. Due to the process being GMAW with pulsed current at different currents, it is difficult to compare with previous work done by McIntosh according to Zhang. As one of the scopes for this work is to work with direct current, it is not going to be compared. One of the following steps of this work, would be to compare the results with Zhangs work, make measurements of that process or study more in detail the theory behind.

Chapter 2

Background

2.1. Gas Metal Arc Welding

The process of GMAW (Gas Metal Arc Welding), uses an inert gas to shield the wire and weld pool from atmospheric contamination. See Figure 2.1 for the GMAW welding equipment components.

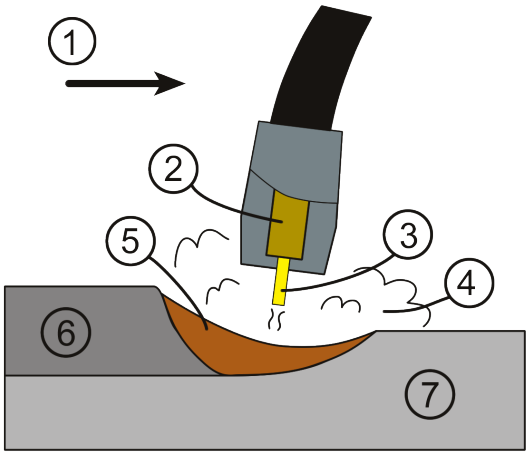

1. Welding direction
2. Contact tip
3. Electrode
4. Shielding gas
5. Welding pool
6. Welded metal
7. Work piece

Figure 2.1: Scheme of process GMAW [7].

The process can be performed with argon, CO_2, helium or a mixture of these inert gases. The wire that is deposited travels through the contact tip and establishes an arc between the electrode extension and the work piece.

2.1.1. Plasma arc

The plasma arc is created because of a voltage differential between two points: the anode and cathode. When this two are close to each other, the potential difference in the air is surpassed and the electricity allows the arc the be generated.

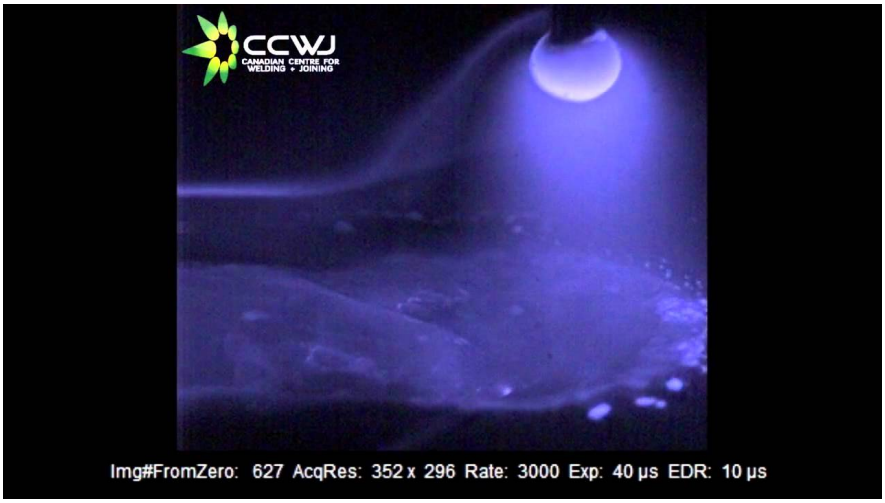

Figure 2.2: Plasma arc generated.

As soon as the electric arc is generated, there is an important amount of heat generated that makes the metal to melt, creating the welding pool as in Figure 2.2. This plasma arc plays an important role on the weld, as it could affect the size of the droplet falling.

2.1.2. Arc column

The arc column is made out of plasma and it generates heat, which is emitted as radiation and convection. The different properties of the plasma depend on the shielding gas being used for the process.

2.1.2.1. Shielding gas

The plasma arc is generated in an environment with air, in this case with argon. When the arc is generated, the temperature is higher than 10000 K, temperature that allows the atoms to dissociate and ionize. The dissociation of argon can be expressed as in equation 2.1. The relation happens at atmospheric pressure.

$$Ar \xrightarrow{\text{ionization}} Ar^{+} + e^{-} \xrightarrow{\text{ionization}} Ar^{2+} + 2e^{-} \tag{2.1}$$

2.1.2.2. Voltage fall

According to J.F. Lancaster [8], the arc column voltage can be expressed as a linear function of the length of it as in equation 2.2.

$$V_{\text{arc}} = \frac{dV}{dl} l_{\text{arc}} \tag{2.2}$$

2.1.3. Anode

The plasma arc that is generated is over 10000 K [9] and the difference in temperature between the arc and the electrode is generated by the fall voltage [8]. The heat generated, is created by the electron movement and the work function of the material. This power loss is expressed as a fall voltage so that it can be an expression related to the current too.

This anode fall voltage in GMAW is the voltage in the electrode, being it the positive pole. The formula for the anode fall voltage is the one to find in almost all literature and also used by McIntosh and Mendez [2]:

$$V_{\text{anode}} = \frac{q_{\text{anode}}}{I} - V_{\text{elec}} - V_{\text{cont}} = \Phi_{\text{anode}} + \frac{3kT}{2e} + V_{\text{anode,sheath}} \tag{2.3}$$

Where Φ_{anode} is the work function of the anode material, k the Boltzmann constant, T the temperature of the electrons, e the charge of electrons and $V_{\text{anode,sheath}}$ the anode sheath voltage generated. To calculate the anode fall voltage, the next table summarises the values obtained for aluminium by the works from McIntosh [4, 2].

Table 2.1: Parameters for anode fall voltage for aluminium.

Φ_{anode} V	T_{e} K	k m^2kg/s^2K	e eV	V_{electron} V	$V_{\text{anode,sheath}}$ V
4,26	6000	1,38 10^{-23}	1,60 10^{-19}	0,78	-0,98 [2]

All the values given were obtained because of the theoretical knowledge around phenomena like this, but those were never measured.

2.1.4. Cathode

In the GMAW process the cathode is the negative pole, being this the plate that is being welded. In this case there are non-thermionic materials, so the power and voltage are the ones as it equation 2.4.

$$V_{\text{cathode}} = V_{\text{cathode, sheath}} - \Phi - \frac{3}{2}\frac{k_{\text{B}}T_{\text{i}}}{e} \tag{2.4}$$

As expressed for the anode fall voltage, this is one item that is expressed in this way so that it can be related to the current too. As the plate is receiving a lot of heat, it is important to acknowledge that the cathode fall heat, could be something similar to equation 2.5.

$$q_{\text{cathode}} = IV_{\text{cathode}} + q_{\text{arc, cathode}} \tag{2.5}$$

The following values from literature were used to calculate the fall voltage, as they appear on the literature [8].

- $V_{\text{cathode, sheath}} \approx 16.7V$ in case of pure Ar y $19.5V$ for Ar$-5\%CO_2$.
- Φ is the work function, being $4.81V$ in Fe and $4.17V$ for Al.

- Also, $\frac{3}{2}\frac{k_B T_i}{e} \approx 11V$ for Ar and $\approx 13.8V$ for Ar$-5\%CO_2$.

These values are usually obtained from theoretical knowledge being one of those made by C. McIntosh and P. Mendez [2].

2.1.5. Other voltages

After understanding the plasma arc, all the other fall voltages must be considered and studied.

2.1.6. Leads

The cables are the way the electricity is carried from the machine until the contact tip. This cables generate a small resistance to the energy and also some impedance to the different pulses. With those two items, the next equations are generated.

$$Z = R + jX \tag{2.6}$$

$$R = \frac{\rho_e l}{A} \tag{2.7}$$

- l: length of the lead.
- A: cross section of the lead.
- $\rho_e = 1.72410^{-8}$ Ωm for Cu.

$$X = 2\pi f L \tag{2.8}$$

The item L is the inductance of the lead, as it is explained by Kraus [10] and it can be expressed as in equation 2.9.

$$L = \frac{\mu_0 l}{2\pi}\left(\ln\frac{4l}{d} - 1\right) \tag{2.9}$$

Being,

- f: wave frequency.
- L: inductance of the conductor.
- $\mu_0 = 4\pi 10^{-7}\Omega s/m$: magnetic permeability of vacuum.
- d: diameter of the lead.

2.1.7. Contact tip

The contact tip is where the cables end and the electrode goes in contact with the shielding gas. Due to the constant movement of the wire, there is a resistance generated. This resistance is considered to be $\sim 2m\Omega$ the best approximation.

2.1.8. Stick out

After the current goes from the lead cable to the electrode, this last one has some length before it gets melted and the plasma arc is generated. The extension of the filler wire, which extends beyond the contact tip, is referred to as the electrode stick out.

2.2. Mass transfer

During the GMAW process, the material deposition is made through a cable that moves with a constant feed speed. This variable with the voltage, are the variables that are controlled in the welding machine by the operator. When the operator changes one variable, the detachment of the droplet can be affected, resulting in globular transfer, spray transfer or short circuit. These different deposition regimes are related to the current and voltage.

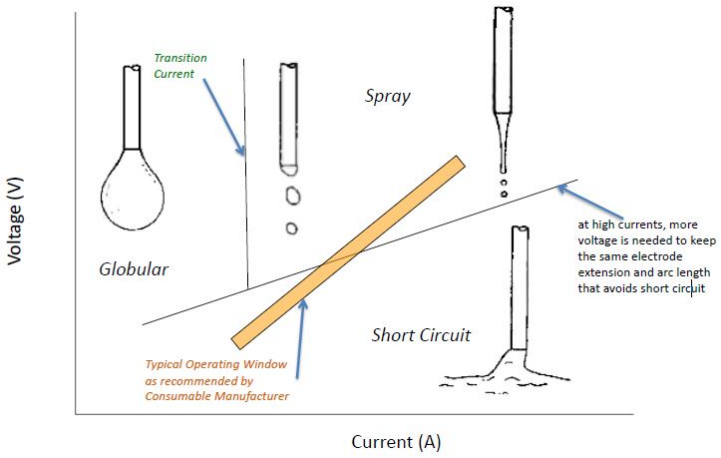

Figure 2.3: Deposition types by P. Mendez.

As can be seen in figure 2.3, there is a transition current between globular and spray transfer. One method to obtain this transition current was developed by John J. Lowke [11] and it is used as a reference.

2.3. Voltage summary

After analysing all the general parameters of the gas metal arc welding process, it is possible to generate the following list of voltages [12].

- Arc column: $0.8 \sim 1V/mm$
- Anode:
  - $\sim 4.8V$ for steel
  - $\sim 4.2V$ for aluminium
- Cathode (non thermoionic):
  - $\sim 11V$ with Ar
  - $\sim 13.8V$ with $Ar - 5\%CO_2$
- Leads:
  - Resistance: $\sim 1V/m$
  - Reactant: $10^{-5}\Omega/(mHz)$
- Contact tip: $2m\Omega$
- Length of stickout: $\sim 0.16V/mm$

There are different ways to obtain the values here presented, either theoretically or experimentally. The way the GMAW process is developed, there is no way yet to measure exactly the anode power loss. This loss is one of the most important, because it contains the droplet temperature and transfer mode. When this power loss is studied as a fall voltage, it is necessary to understand all the details of it.

Chapter 3

Methodology

At the beginning of the work, all the data from the experimeadnts done was alrey available from a previous work performed at the CCWJ, but the theory behind the anode fall voltage and droplet evaporation needed to be revisited. A previous work by professor Ph.D. Mendez was realized, but it did not contain the calculation of the anode fall voltage and the evaporation was considering a solution of steel and manganese. This work contained a lot of values that were assumed to be real, but were not calculated. That is how this work started, by understanding all the previous work done and by developing a model out of the energy balance. All the values and formulas were revisited, calculated and backgrounded.

The energy balance was already performed in different ways, but some assumptions regarding the heat stored or the metal evaporated were different. These two points were a key point to study: the evaporation needed to be considered and it is going to be assumed that there is no heat stored on the control volume. Due to the steady state, out of a cyclic state, it is assumed that there is no heat stored.

This thesis aims to develop an energy balance on the electrode and droplet of the GMAW welding and by that have an expression to calculate the anode fall voltage of the process. The evaporation model was also considered to be done, as it is not known exactly what percentage of the droplet to consider, either for the mass or energy balance. According to the scopes of this work, the following assumptions were used:

- Steady state model, due to the cyclic process.
- Sphere droplets.
- No heat losses due to radiation over the droplet or electrode stick out.
- Constant composition of the electrode over time.

With this assumptions it is possible to expect a decent model that could show the dependence of the anode fall voltage to another variable. As it could be the current, it also should be able to show the importance of the mass evaporated and the heat that is lost due to it. It is not the aim of this work to develop a sensitivity analysis of each variable, but to be able to understand how it could affect on the overall balance.

3.1. Data acquisition

The measurements that were made to obtain the different droplet temperatures were made by a previous student at the CCWJ laboratory. This data acquisition was made to obtain the droplet temperatures at different currents with electrodes of various compositions. The equipment used is the same as utilized by C. McIntosh and P. Mendez in article [2] and can be seen in Figure 3.1.

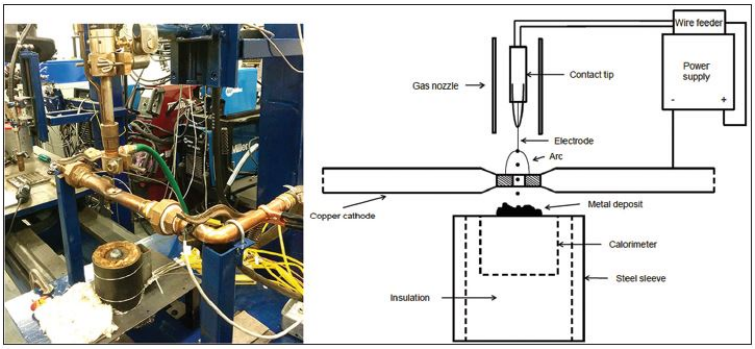

Figure 3.1: Experiment set-up by McIntosh.

The GMAW arc is generated over a copper cathode tube that has flowing water inside. There is a hole in the middle of this tube, where the arc is generated, that allows the droplet to fall through and over a calorimeter. After analysing this system is possible to obtain the droplet average temperature out of the calorimeter and the heat generated on the cathode, matching the temperatures with the current, voltage and WFS of the measurement. The data was sampled and saved on different videos, where it is possible to see the droplet fall and the behaviour of the current and voltage at the same time, as can be seen in figure 3.2.

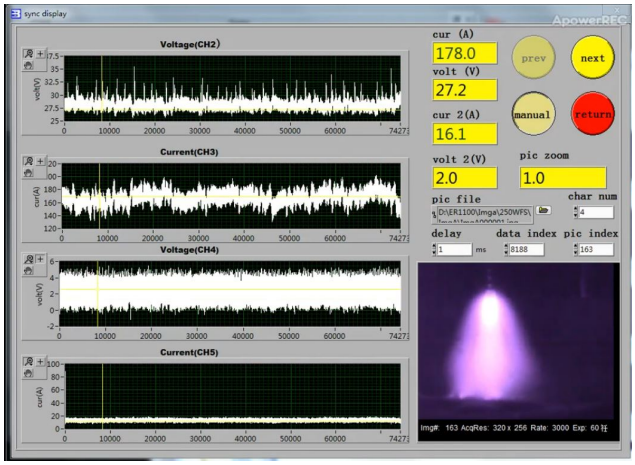

Figure 3.2: Results obtained from measurements performed.

For the experiments performed the main target was to get the droplet temperature related to different currents. For this, some variables were hold stable and changed the other ones. The first variable to maintain constant was the gas mix used, that was pure argon and only used with direct current and electrode positive. In this case the CTWD (electrode extension

plus arc length) was also constant, as figure 3.3 shows. Every one of them was meant to stay at 12,5 mm as also the current, while varying the other variables: voltage and WFS. These two were constantly changed while monitoring the current of the process and trying to stabilize the arc at the given electrode extension. When the current and the electrode extension were obtained at the desired values, the droplet was allowed to fall to the calorimeter and the recording started. This process was repeated for current values from globular into spray transfer and for different electrodes.

Figure 3.3: Contact tip and arc length used.

Chapter 4

Work done

4.1. Energy balance in electrode extension

In the GMAW process, the droplet from the electrode receives from different sources heat and also gives away. When it is studied in steady state, there is no heat stored. The control volume for the balance is shown in Figure 4.1 and Equation 4.1 is the heat balance that describes the system. It is important to acknowledge that the control volume considers the thickness of the diffusion boundary layer over the melted droplet.

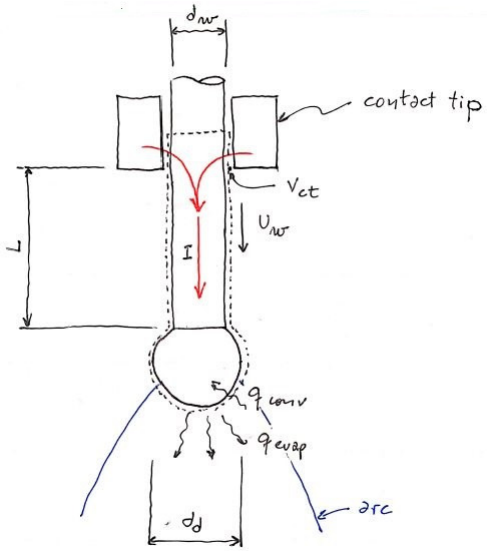

Figure 4.1: Control volume studied.

$$q_{\text{in}} - q_{\text{out}} + q_{\text{gen}} = q_{\text{st}} = 0 \tag{4.1}$$

First of all is the heat that enters control the volume q_{in}:

$$q_{\text{in}} = q_{\text{fall}} + q_{\text{arc}} + q_{\text{ct}} + q_{\text{adv,in}} \tag{4.2}$$

Being every item:

$$q_{\text{fall}} = IV_{\text{fall}} \tag{4.3}$$
$$q_{\text{arc}} = h_{\text{arc,elec}} A_{\text{anode}} (T_{\text{ion}} - T_{\text{d}}) \tag{4.4}$$
$$q_{\text{ct}} = R_{\text{ct}} I^2 \tag{4.5}$$
$$q_{\text{adv,in}} = \dot{m}_{\text{c}} i_0 \tag{4.6}$$

The term q_{arc} is approximately 1% of the heat from the energy balance done by Quigley [13], but it is calculated as in Equation 4.4. It is assumed that the droplet receives heat as convection from the arc as by Lehnhoff [14] and just into the down side of the droplet, an area characterized with the anode spot radius. Temperature T_{ion} is the ionization temperature of the shielding gas and A_{anode} is the area of the anode spot 4.7 and the convection coefficient is explained in Equation 4.8.

$$A_{\text{anode}} = \frac{I}{\pi J_{\text{a}}} \tag{4.7}$$
$$h_{\text{arc,elec}} = \frac{k_{\text{int}} \text{Nu}_{\text{heat}}}{D_{\text{d}}} \tag{4.8}$$

The term k_{int} is the thermal conductivity of Argon, J_{a} is the current density at the anode and Nu_{heat} is the Nusselt number of the process.

$$\text{Nu}_{\text{heat}} = 2 + 0,6 \text{Re}^{0,5} \text{Pr}^{1/3} \tag{4.9}$$
$$\text{Re} = \frac{\rho_{\text{Ar}} v_{\text{Ar}} D_{\text{d}}}{\mu_{\text{Ar}}} \tag{4.10}$$
$$\text{Pr} = \frac{\mu_{\text{Ar}} c_{\text{p}}^{Ar}}{k_{\text{Ar}}} \tag{4.11}$$

The heat that goes out of the control volume q_{out} and what is generated q_{gen} are:

$$q_{\text{out}} = \dot{m}_{\text{d}} i_{\text{d}} + \dot{m}_{\text{g}} i_{\text{g}} \tag{4.12}$$
$$q_{\text{gen}} = \frac{I^2 L \rho_{\text{eff}}}{A_{\text{e}}} \tag{4.13}$$

Looking at the mass that goes in and out, there is a balance between the mass from the wire (in), the droplet that falls and the mass evaporated (out). This can be expressed in the next equation.

$$\dot{m}_{\text{c}} = \dot{m}_{\text{d}} + \dot{m}_{\text{g}} \tag{4.14}$$

Replacing every item in the original equation:

$$q_{\text{fall}} + q_{\text{arc}} + q_{\text{ct}} + \frac{I^2 L \rho_{\text{eff}}}{A_{\text{e}}} + \dot{m}_{\text{c}} i_0 - (\dot{m}_{\text{d}} i_{\text{d}} + \dot{m}_{\text{g}} i_{\text{g}}) = 0 \tag{4.15}$$

The mass evaporated from the droplet is calculated according to Equation 4.16.

$$\dot{m}_\mathrm{g} = JMA_\mathrm{d} \tag{4.16}$$

$$\dot{m}_\mathrm{c} = U_\mathrm{c} m'_\mathrm{c} \tag{4.17}$$

Replacing items and erasing others:

$$V_\mathrm{fall} I + R_\mathrm{ct} I^2 + \frac{I^2 L \rho_\mathrm{eff}}{A_\mathrm{e}} + q_\mathrm{arc} + \dot{m}_\mathrm{c}\left(i_0 - i_\mathrm{g}\right) + \dot{m}_\mathrm{d}\left(i_\mathrm{d} - i_\mathrm{g}\right) = 0 \tag{4.18}$$

4.2. Wire Feed Speed

Out of Equation 4.18 it is possible to obtain the WFS U_c of the process.

$$U_\mathrm{c} = \frac{V_\mathrm{fall} I + I^2\left[R_\mathrm{ct} + \frac{L\rho_\mathrm{eff}}{A_\mathrm{e}}\right] + q_\mathrm{arc} + \dot{m}_\mathrm{d}\left(i_\mathrm{g} - i_\mathrm{d}\right)}{m'_\mathrm{c}\left(i_\mathrm{g} - i_0\right)} \tag{4.19}$$

Analysing the enthalpy on a different way:

$$i_\mathrm{g} - i_0 = (i_\mathrm{g} - i_\mathrm{d}) + (i_\mathrm{d} - i_0) = \Delta i_\mathrm{lg} + \Delta i_\mathrm{ref} + c_\mathrm{p}(T_\mathrm{d} - T_\mathrm{ref,l}) + c_\mathrm{p}(T_\mathrm{g} - T_\mathrm{d}) \tag{4.20}$$

When replacing every item on Equation 4.19 and where $\dot{m}_\mathrm{d}$ can be broken down to 4.21, the expression for the WFS is as Equation 4.22 shows.

$$\dot{m}_\mathrm{d} = \dot{m}_\mathrm{c} - \dot{m}_\mathrm{g} \tag{4.21}$$

$$U_\mathrm{c} = \frac{V_\mathrm{fall} I + I^2\left[R_\mathrm{ct} + \frac{L\rho_\mathrm{eff}}{A_\mathrm{e}}\right] + q_\mathrm{arc} + (\dot{m}_\mathrm{c} - \dot{m}_\mathrm{g})(\Delta i_\mathrm{lg} + c_\mathrm{p}(T_\mathrm{g} - T_\mathrm{d}))}{m'_\mathrm{c}\Big[\Delta i_\mathrm{lg} + \Delta i_\mathrm{ref} + c_\mathrm{p}(T_\mathrm{d} - T_\mathrm{ref,l}) + c_\mathrm{p}(T_\mathrm{g} - T_\mathrm{d})\Big]} \tag{4.22}$$

4.3. Anode fall voltage

Out of Equation 4.23 it is possible to isolate the anode fall voltage IV_{anode} as in Equation 4.24 and then replace every item of enthalpy.

$$IV_{\text{fall}} + R_{\text{ct}} I^2 + \frac{I^2 L \rho_{\text{eff}}}{A_{\text{e}}} + q_{\text{arc}} - \dot{m}_{\text{d}} i_{\text{d}} - \dot{m}_{\text{g}} i_{\text{g}} + \dot{m}_{\text{c}} i_0 = 0 \tag{4.23}$$

$$IV_{\text{fall}} = \dot{m}_{\text{c}} \left(i_{\text{d}} - i_0\right) + \dot{m}_{\text{g}} \left(i_{\text{g}} - i_{\text{d}}\right) - R_{\text{ct}} I^2 - \frac{I^2 L \rho_{\text{eff}}}{A_{\text{e}}} - q_{\text{arc}} \tag{4.24}$$

The terms of enthalpy should be written on a different way, so that it contains all the phase changes on the process.

$$i_{\text{d}} - i_0 = \Delta i_{\text{ref}} + c_{\text{p}} \left(T_{\text{d}} - T_{\text{ref,liq}}\right) \tag{4.25}$$

$$i_{\text{g}} - i_{\text{d}} = \Delta i_{\text{liq,gas}} + c_{\text{p}} \left(T_{\text{g}} - T_{\text{d}}\right) \tag{4.26}$$

The term Δi_{ref} contains the enthalpy from room temperature until the liquid state. Also the term $\dot{m}_{\text{c}}$ can be written in terms of the WFS and linear mass flow.

$$IV_{\text{fall}} = U_{\text{c}} m'_{\text{c}} \left(\Delta i_{\text{ref}} + c_{\text{p}} \left(T_{\text{d}} - T_{\text{ref,liq}}\right)\right) + \dot{m}_{\text{g}} \left(\Delta i_{\text{liq,gas}} + c_{\text{p}} \left(T_{\text{g}} - T_{\text{d}}\right)\right) - R_{\text{ct}} I^2 - \frac{I^2 L \rho_{\text{eff}}}{A_{\text{e}}} - q_{\text{arc}} \tag{4.27}$$

4.3.1. Resistivity

During the welding process, the droplet is at melting temperature, while it entering the control volume at room temperature. This big difference on just a few millimetres on the wire, causes an important change of resistivity. As in article made by Lehnhoff and Mendez [14] the resistivity is calculated for the GMAW process. This model includes the conduction and Joule heating effects, while considering losses by convection and radiation, within others.

$$\rho_{\text{eff}} = \frac{H_{\text{C2}}^{+*} H_{\text{c}} \dot{m}_{\text{c}} A_{\text{e}}}{L I^2} \tag{4.28}$$

Being H_{c} the difference in enthalpy from room temperature until the droplet temperature. The item H_{C2}^{+*} is the normalized improved enthalpy increase and it can be calculated as Equation 4.29.

$$H_{\text{C2}}^{+*} = \frac{2(e^{d/M_1} - 1)}{b(1 - e^{d/M_1}) + d(1 + e^{d/M_1})} \tag{4.29}$$

Being every item,

$$d = \sqrt{b^2 - 4a} \tag{4.30}$$

$$b = \frac{\Delta\rho_1}{\rho_0} + 4\frac{\Delta\rho_2}{\rho_0} \tag{4.31}$$

$$a = -4\frac{\Delta\rho_2}{\rho_0} \tag{4.32}$$

$$M_1 = \frac{U_\mathrm{c} H_\mathrm{c} A_\mathrm{e}^2}{L\rho I^2} \tag{4.33}$$

The value of ρ_0 is the electrical resistivity at room temperature, ρ_s is the electrical resistivity at the solidus temperature, where the melting starts. This value was obtained using Equation 4.34 from [14].

$$k_\mathrm{s}\rho_\mathrm{s} = \frac{\pi^2 k_\mathrm{b}^2}{3e^2} T_\mathrm{s} \tag{4.34}$$

Being k_s the heat conductivity and T_s the temperature at melting temperature. With those values, the next ones can be calculated:

$$\Delta\rho_1 = \rho_\mathrm{m} - \rho_0 \tag{4.35}$$

$$\Delta\rho_2 = \rho - \rho_0 + \frac{\Delta\rho_1}{H_\mathrm{c}}(i_\mathrm{d} - i_0) \tag{4.36}$$

4.4. Mass evaporated

During the GMAW process there are different sources of metal evaporation. The two areas are the ones that are melted: the welding pool and the droplet. In this case only the droplet evaporation is going to be explained, as is the one on the control volume.

Out of Ficks second law, it is possible to write Equation 4.37 as the mass transfer of the droplet due to vaporization.

$$\dot{m}_{\mathrm{g}} = \dot{m}''_{\mathrm{g}} A_{\mathrm{d}} = JMA_{\mathrm{d}} \tag{4.37}$$

Being $\dot{m}''_{\mathrm{g}}$ the evaporation rate per area of the droplet, A_{d} the surface area of the droplet, M the molar weight of the electrode and J the equivalent of $\dot{m}''_{\mathrm{g}}$, but per mole.

4.4.1. Area of the droplet

Considering the droplet as a sphere, being D_{d} the droplet diameter and d_{c} the wire diameter, the volume and area are:

$$A_{\mathrm{d}} = \pi(D_{\mathrm{d}}^2 - \frac{d_{\mathrm{c}}^2}{4}) \tag{4.38}$$

$$V_{\mathrm{d}} = \frac{1}{6}\pi D_{\mathrm{d}}^3 \tag{4.39}$$

If the transfer mechanism is spray transfer, usually the droplet diameter is smaller than the electrode diameter. In this case the electrode diameter is not considered for Equation 4.38.

4.4.2. Diameter of the droplet

As in one publication from Lowke [11], it is possible to obtain different relationships for the droplet detachment out of a mass balance. A small part of that work has been studied, but as it seems to not work properly, it is just going to be explained for future considerations.

4.4.2.1. Based on Lowke's work

To obtain the droplet diameter, it is necessary to make a balance of forces at the moment of detachment of the droplet from the wire, as it can be seen in Equation 4.40. The forces that are pushing for the droplet to detach are the gravity (4.41), the electromagnetic (4.42) force and the drag of the gas over the droplet. On the other side, pulling it back, are the surface tension (4.43) and the electromagnetic force of the arc. The electromagnetic force and the drag, both pushing the droplet down, are negligible due to their magnitude compared to the others [11].

$$P_{\text{surf}} = P_{\text{g}} + P_{\text{em}} \tag{4.40}$$

$$P_{\text{g}} = \frac{1}{2}\rho g D_{\text{d}} \tag{4.41}$$

$$P_{\text{em}} = \frac{\mu_0 I^2}{\pi^2 d_{\text{c}}^2} \tag{4.42}$$

$$P_{\text{surf}} = \frac{4\gamma}{d_{\text{c}}} \tag{4.43}$$

When using Equations 4.43, 4.42, 4.41 and 4.40, by solving for D_{d} it is possible to get Equation 4.44.

$$D_{\text{d}} = \sqrt[3]{\frac{12}{\rho g \pi}\left(\frac{4\gamma}{d_{\text{c}}} - \frac{\mu_0 I^2}{\pi^2 d_{\text{c}}^2}\right)} \tag{4.44}$$

4.4.2.2. Empirical analysis

Another way to calculate the droplet diameter is by an empirical analysis. Assuming a droplet frequency f of detachment and that the the mass entering the system is the same as the mass that leaves (no evaporation), Equation 4.45 can be expressed.

$$D_{\text{d}} = \sqrt[3]{\frac{6\dot{m}_{\text{c}}}{\pi \rho f}} \tag{4.45}$$

4.4.3. Molar concentration difference

It can be assumed out of the ideal gas law [15], that it is possible to describe the molar concentration difference of the droplet surface. The value of J is obtained for every material and then condensed into one according to the molar fraction of the electrode.

$$J = \frac{P_{\text{v}}}{R T_{\text{d}}} \frac{1}{R''_{\text{tot}}} \tag{4.46}$$

Being R'' the analogy of a resistance for mass transfer, R the ideal gases constant, T_{d} the droplet temperature and P_{v}^j the vapour pressure for each material, as it varies on every material, as done by Alcock *et al.* [16]. The values obtained for Si were obtained out of a linear tendency from the CRC Handbook of Chemistry and Physics [17].

$$\log\left(P_{\text{v}}^j\right) = A + \frac{B}{T_{\text{d}}} + C\log(T_{\text{d}}) + D T_{\text{d}} 10^{-3} \tag{4.47}$$

$$P_{\text{v}}^{Si} = A \ln T_{\text{d}} + B \tag{4.48}$$

In the case when the boiling temperature of one component is below the droplet temperature, the vapour pressure has to consider a reduction of one atmosphere $P_{\text{v}} - P_{\text{atm}}$. This happens because when the element starts to boil, it goes out of the droplet and the boundary layer is moved to the outside.

Table 4.1: Parameters for vapour pressure for each component.

Component (j)	A	B	C	D	Reference
Fe	6,347	-19574			[16]
Al	10,578	-16946	-1,3133		[16]
Mg	8,489	-7813	-0,8253		[16]
Mn	12,805	-15097	1,7896		[16]
Cr	6,8	-20733	0,43991	-0,4094	[16]
Cu	11,209	17427	-1,4742		[16]
Zn	5,378	-6286			[16]
Si	121,84	1569,4			[17]

4.4.4. Mass transfer resistance

In this case the therm is R''_{tot} that is the total resistance to vaporization of the material per area of the droplet. Due to the control volume definition, this resistance can be decomposed in two therms: the surface resistance to vaporization as by Langmuir's evaporation in Equation 4.50 and the boundary layer of vapour over the droplet in equation 4.51.

$$R''_{\text{tot}} = R''_{\text{surface}} + R''_{\text{BL}} \tag{4.49}$$

$$R''_{\text{surface}} = \sqrt{\frac{2\pi M}{RT_{\text{d}}}} \tag{4.50}$$

$$R''_{\text{BL}} = \frac{1}{h_{\text{BL}}} \tag{4.51}$$

In this case being M the molecular mass of the electrode, R the universal constant of gases, m_{d} the mass and T_{d} the temperature of the droplet. When the boiling temperature of one element is below the droplet temperature, the boiling temperature is used for the calculations. The therm h_{BL} is the resistance at the boundary layer, that is expressed in Equation 4.52.

$$h_{\text{BL}} = \frac{Sh_{\text{D}}D}{D_{\text{d}}} \tag{4.52}$$

The value of h_{BL} depends on the geometry, affecting directly the Sherwood number Sh_{D}. Also it considers a sphere of diameter D_{d} with a diffusivity D of the material on a gas phase.

4.4.4.1. Dimensionless numbers

To calculate Equation 4.52 it is necessary to obtain the Sherwood number 4.53.

$$Sh_{\text{D}} = 2 + 0,6Re_{\text{D}}^{0,5}Sc^{1/3} \tag{4.53}$$

Being Re_{D} the Reynolds number and Sc the Schmidt number, both for a droplet of diameter D and surrounded by argon in plasma conditions.

$$Re_{\mathrm{D}} = \frac{\rho_{\mathrm{Ar}} v_{\mathrm{Ar}} D_{\mathrm{d}}}{\mu_{\mathrm{Ar}}} \tag{4.54}$$

$$Sc = \frac{\mu_{\mathrm{Ar}}}{\rho D} \tag{4.55}$$

In this case, the physical properties for the argon are at the plasma temperature $T = 7200$ K near the droplet. The droplet diameter is D_{d} and D is the gas diffusivity for the electrode material. The velocity v is calculated as by P. Mendez in [18].

$$v = \frac{1}{2}\sqrt{\frac{\mu_0}{\rho_{\mathrm{max,T}}}} J_{\mathrm{a}} r_{\mathrm{a}} f_{\mathrm{VZ}} \tag{4.56}$$

$$r_{\mathrm{a}} = \frac{I}{J_{\mathrm{a}} \pi} \tag{4.57}$$

The value of r_{a} is the anode spot radius, that is considered to change with the current, but keeping the current density J_{a} constant, based on the values used by Soderstrom [19].

According to Mendez [18] a correction factor is necessary for the plasma velocity 4.58.

$$f_{\mathrm{VZ}} = 0,55 Re_{\mathrm{h}}^{0,073} \left(\frac{h}{r_{\mathrm{a}}}\right)^{0,0068} \tag{4.58}$$

In this case the Reynolds number is calculated according to the arc length and with the properties of argon on plasma phase.

4.4.5. Diffusivity

As by the theory developed by Poirer [20], with the Chapman-Enskog equations, the diffusivity can be calculated as by Equation 4.59. The different values obtained for diffusivity are for one material (j) from the electrode over argon.

$$D = \frac{AT^{3/2}}{p\sigma^2 \Omega} \left(\frac{1}{M_{\mathrm{Ar}}} + \frac{1}{M_{\mathrm{j}}}\right) \tag{4.59}$$

The value of $A = 0,0018583$ is to give the value of diffusivity in (cm^2/s). The value of Ω is developed by Reid *et al.* [21] and is calculated by the Equation 4.60:

$$\Omega = \frac{1,06036}{T^{*0,1261}} + \frac{0,193}{\exp(0,47633 T^*)} + \frac{1,03587}{\exp(1,52996 T^*)} + \frac{1,76474}{\exp(3,89411 T^*)} \tag{4.60}$$

Being T^* the value of a dimensionless temperature, that can be calculated as Equation 4.61 developed by Turkdogan *et al.* [22].

$$T^* = \frac{kT}{\epsilon_{\mathrm{AB}}} \tag{4.61}$$

$$\epsilon_{\mathrm{AB}} = \sqrt{\epsilon_{\mathrm{A}} \epsilon_{\mathrm{B}}} \tag{4.62}$$

$$\sigma_{12} = \frac{\sigma_1 + \sigma_2}{2} \tag{4.63}$$

4.5. Different droplet temperatures

Different works studies include the measurements of droplet temperatures. This ones were obtained with the parameters needed to obtain more anode fall voltages and mass evaporated.

4.5.1. Measurements by K. Scott

The work by K. Scott [23] has measurements of droplet temperature for a ER70S-G electrode. The data obtained from this work is shown in Table 4.2.

Table 4.2: Values from Scott.

Current A	WFS m/s	Droplet Temp. $°C$
181,1	0,086	2261
188,1	0,090	2380
188,7	0,090	2434
195,9	0,095	2444
197,8	0,096	2375
205,0	0,100	2356
206,9	0,101	2418
208,1	0,102	2513
215,3	0,106	2447
217,8	0,107	2604
228,1	0,114	2596
232,0	0,116	2601
234,6	0,117	2577

4.5.2. Measurements by E. Soderstrom

The work by E. Soderstrom [19] has measurements of droplet temperature for ER70S-G and ER4043 electrodes. The data obtained from this work is shown in Tables 4.3 and 4.4.

Table 4.3: Values for ER4043 from Soderstrom.

Current A	WFS m/s	Droplet Temp. $°C$
85	0,055	1962,4
100	0,065	1990,0
107	0,069	2017,5
118	0,077	2045,0
134	0,087	2072,6
146	0,095	2100,1
149	0,097	2127,6
165	0,107	2155,2
170	0,110	2182,7
181	0,118	2210,2
195	0,127	2237,8
221	0,144	2265,3

Table 4.4: Values for ER70S-G from Soderstrom.

Current A	WFS m/s	Droplet Temp. $°C$
185,1	0,088	2055
186,1	0,089	2204
189,1	0,091	2460
197,1	0,095	2440
202,1	0,098	2246
204,2	0,099	1990
210,1	0,103	2222
214,1	0,105	2363
217,2	0,107	2375
227,2	0,113	2421
230,0	0,115	2326
247,9	0,125	2581
251,2	0,127	2490
255,0	0,129	2473
257,2	0,131	2666
261,1	0,133	2540

4.6. Data used

The data then used contained the following variables for each electrode: wire diameter, welding current, WFS, electrode extension, roll temperature, ambient pressure, voltage contact tip, total voltage and droplet temperature as can be seen in Appendix A. All the material properties from the electrode or from argon have to be revisited before the calculations were made.

The main software used for the calculations was *Excel*. The different values of enthalpy of electrodes were obtained mainly by the software *JMatPro* and when not available on it, under the corresponding literature. The data used for argon was obtained out of measurements previously done in the laboratory. Some calculations, like the diffusivity, need specific values to calculate it, reason why values were obtained from publications. In the case of the droplet diameter, the frequency used was obtained from the videos of the measurements, but when not available $f = 30\ Hz$ was used. For the calculations of the plasma arc, an optimization was made. The Reynolds number used for the correction factor, used a velocity near 300 m/s. After calculating the velocity the *Solver* extension was used to make the two velocities converge to be the same.

The different electrodes that were used are the ones available in the data acquisition and the ER70S-G was used to compare results with droplet temperatures from different works. The electrodes composition can be seen in Appendix B.

The enthalpies used can be seen on Appendix C. This values were obtained in every material for every 5 °C under the range of 20°C and the boiling temperature. After obtaining all the data, a table was generated with the data at the key temperatures: room, solidification, liquid, reference (1500 or 2000 °C) and boiling temperature. The enthalpy at droplet temperature was extrapolated between the reference temperature and boiling temperature. All the other physical properties were obtained in the same way.

The data used for the argon properties was obtained from a work done by Tony Murphy that was shared with the laboratory. Out of a work done in the laboratory, the resistance of the contact tip obtained and used was $R_{\mathrm{CT}} = 0,002\ \Omega$.

Chapter 5

Results

The calculations from the above section were made for every measurement of the different droplet temperatures performed previously for different electrodes. The anode fall voltage is calculated for every current, as also the mass evaporated out of the droplet and the WFS of every point, behaviour that can be seen in the graphs that follow.

5.0.1. Voltage and evaporation per electrode

The data used goes from low to high currents, what means that goes from globular to spray transfer. All the currents, anode fall voltages, anode heat and mass evaporated are shown in the different tables for each electrode.

5.0.1.1. ER1100

For the electrode ER1100 the data is shown in Table 5.1. This table contains for every current measured the results for the anode fall voltage, the heat on the anode, the mass evaporated and the rate between the anode fall voltage and the total voltage of the measurement.

When the above data is plotted, the following two figures can be obtained.

From Equation 4.22 it is possible to plot the WFS and the current to compare it with the recommendation given by the Lincoln GMAW Brochure.

Table 5.1: General results for ER1100.

I A	V_{anode} V	Q_{anode} W	Evap. %	$V_{\text{anode}}/V_{\text{total}}$ %
99,32	5,37	533,42	0,50%	22,37%
103,22	5,65	582,84	0,54%	22,51%
115,52	4,94	570,39	0,49%	20,40%
120,48	4,40	530,16	0,10%	17,28%
121,79	4,78	581,70	0,12%	18,48%
141,04	4,39	618,79	0,11%	16,86%
142,90	5,12	732,04	0,39%	19,33%
143,83	5,22	751,50	0,32%	19,42%
158,35	5,03	797,29	0,37%	18,48%
168,10	5,07	851,76	0,48%	18,37%
170,15	5,17	879,16	0,44%	18,36%
202,38	5,35	1081,88	0,14%	17,84%
226,73	5,36	1215,32	0,70%	17,13%
237,71	6,00	1425,37	0,85%	19,32%

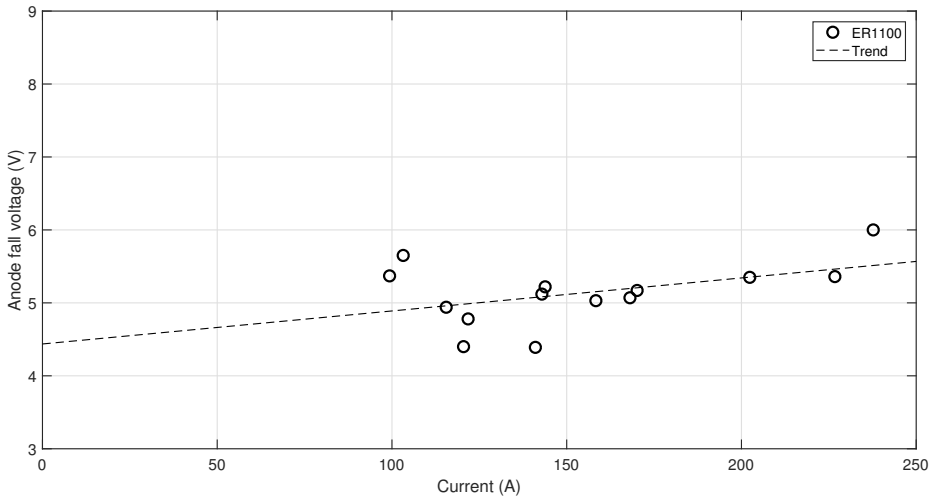

Figure 5.1: Anode fall voltage and current for ER1100.

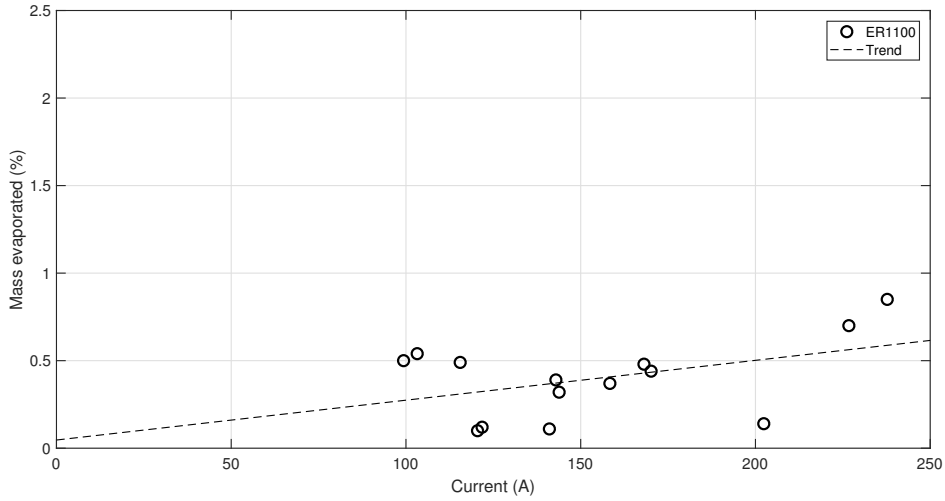

Figure 5.2: Evaporation percentage and current for ER1100.

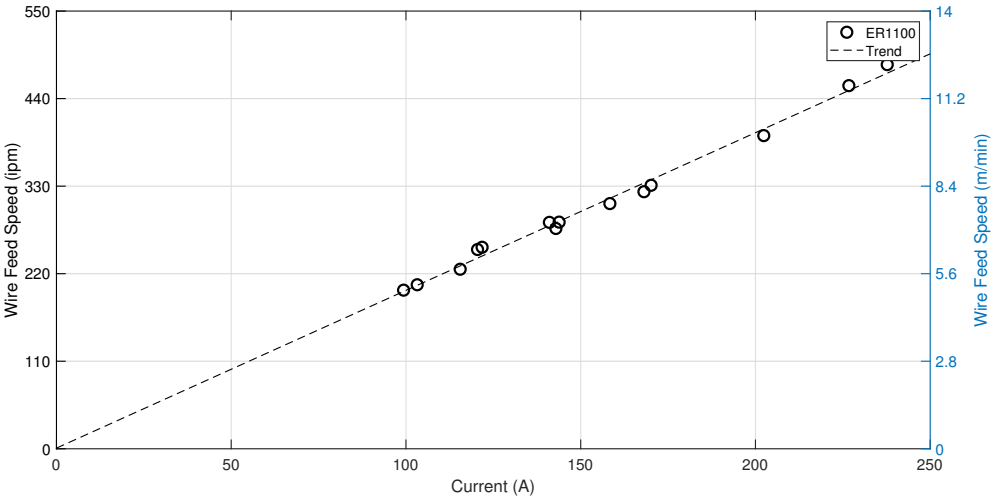

Figure 5.3: Wire feed speed and current for ER1100.

5.0.1.2. ER4043

For the electrode ER4043 the data is shown in Table 5.2. This table contains for every current measured the results for the anode fall voltage, the heat on the anode, the mass evaporated and the rate between the anode fall voltage and the total voltage of the measurement.

Table 5.2: General results for ER4043.

I A	V_{anode} V	Q_{anode} W	Evap. %	$V_{\text{anode}}/V_{\text{total}}$ %
81,30	5,57	452,94	0,12%	18,59%
96,20	5,40	519,92	0,14%	20,60%
105,80	5,48	579,97	0,24%	20,45%
124,50	4,79	596,48	0,20%	17,75%
130,20	5,13	667,60	0,34%	18,50%
136,40	4,65	633,85	0,09%	16,37%
138,10	4,58	632,29	0,05%	15,98%
148,10	4,69	695,09	0,14%	16,01%
144,40	5,80	838,00	0,36%	22,33%
153,30	5,54	848,88	0,51%	21,22%
161,00	5,17	831,89	0,25%	19,50%
159,70	5,61	895,86	0,22%	20,86%
185,92	4,65	863,65	0,29%	17,15%
190,11	4,75	903,77	0,26%	17,47%
204,12	4,96	1012,23	0,40%	17,77%
214,09	4,79	1025,23	0,06%	16,93%
235,65	5,16	1214,94	1,35%	17,48%

When the above data is plotted, the following two figures can be obtained.

From Equation 4.22 it is possible to plot the WFS and the current to compare it with the recommendation given by the Lincoln GMAW Brochure.

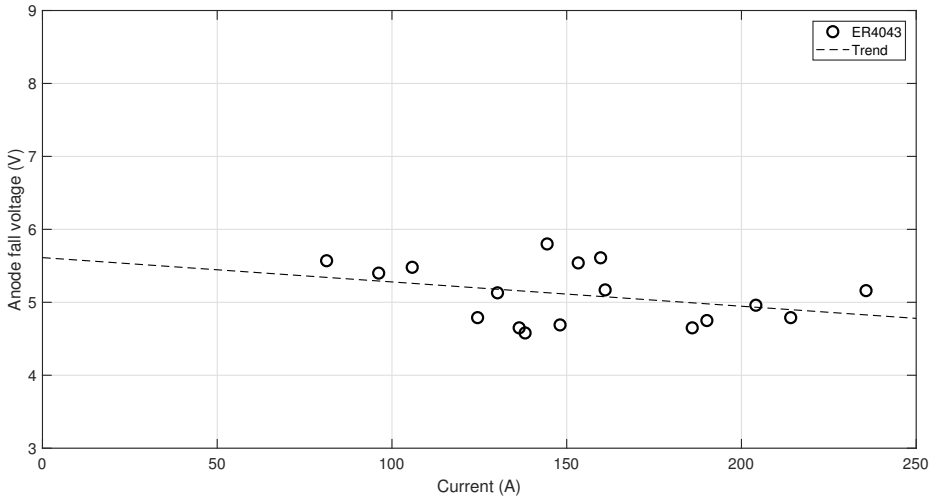

Figure 5.4: Anode fall voltage and current for ER4043.

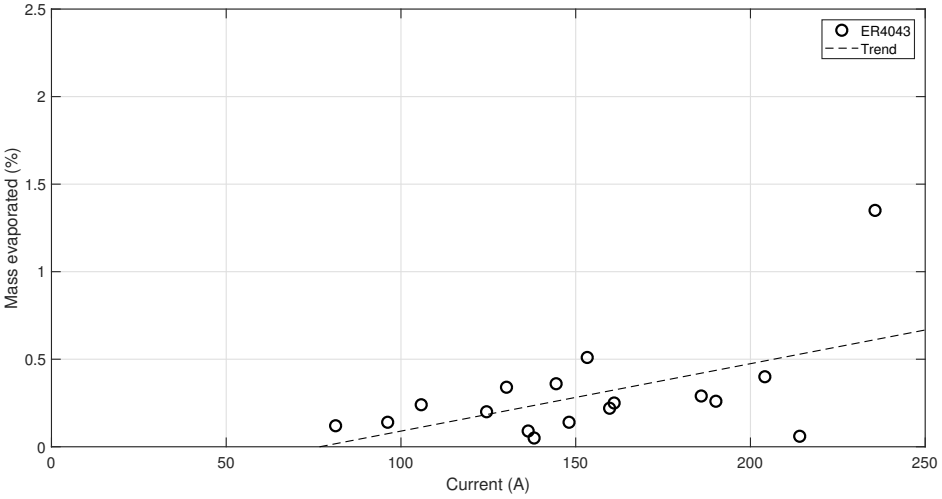

Figure 5.5: Evaporation percentage and current for ER4043.

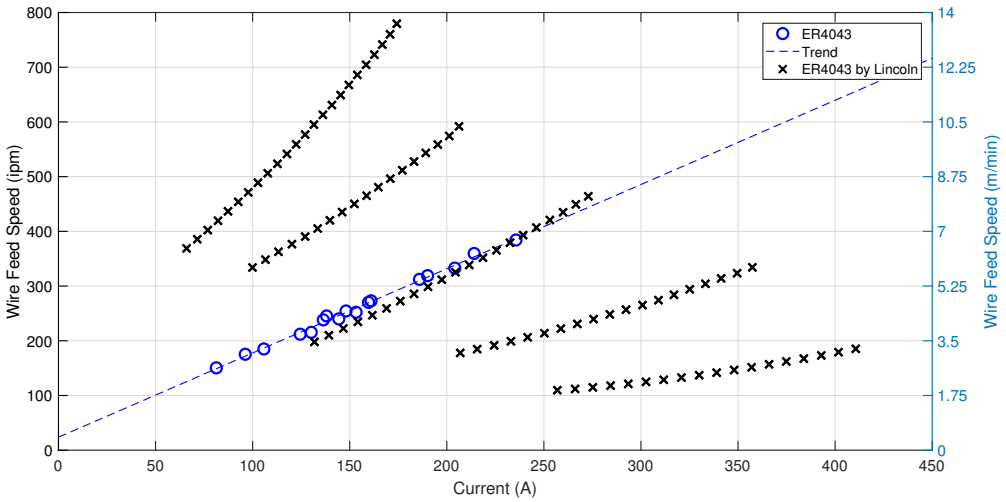

Figure 5.6: Wire feed speed and current for ER4043.

5.0.1.3. ER5554

For the electrode ER5554 the data is shown in Table 5.3. This table contains for every current measured the results for the anode fall voltage, the heat on the anode, the mass evaporated and the rate between the anode fall voltage and the total voltage of the measurement.

Table 5.3: General results for ER5554.

I A	V_{anode} V	Q_{anode} W	Evap. %	$V_{\text{anode}}/V_{\text{total}}$ %
67,93	6,27	425,77	1,72%	26,45%
70,37	6,82	479,60	1,71%	28,16%
82,16	6,74	553,67	1,68%	26,96%
88,39	7,09	626,40	1,88%	27,92%
122,84	5,89	723,63	1,46%	22,90%
125,30	5,68	711,88	0,74%	21,78%
128,46	5,45	699,69	0,40%	20,56%
131,68	5,62	740,03	0,34%	20,89%
135,46	5,95	805,76	0,38%	21,83%
140,60	6,22	875,15	0,48%	22,53%
146,56	6,34	929,26	0,54%	22,77%
150,46	6,20	933,46	0,36%	22,14%
155,07	6,25	969,10	0,34%	22,16%
163,19	6,34	1033,85	0,31%	22,10%
171,85	6,17	1060,43	0,19%	21,18%
184,19	6,42	1182,50	0,28%	21,76%
198,41	5,91	1172,33	0,15%	19,85%
208,80	6,01	1255,69	0,17%	20,01%
215,06	6,33	1361,59	0,21%	20,85%
231,61	5,84	1351,76	0,14%	19,11%

When the above data is plotted, the following two figures can be obtained.

From Equation 4.22 it is possible to plot the WFS and the current to compare it with the recommendation given by the Lincoln GMAW Brochure.

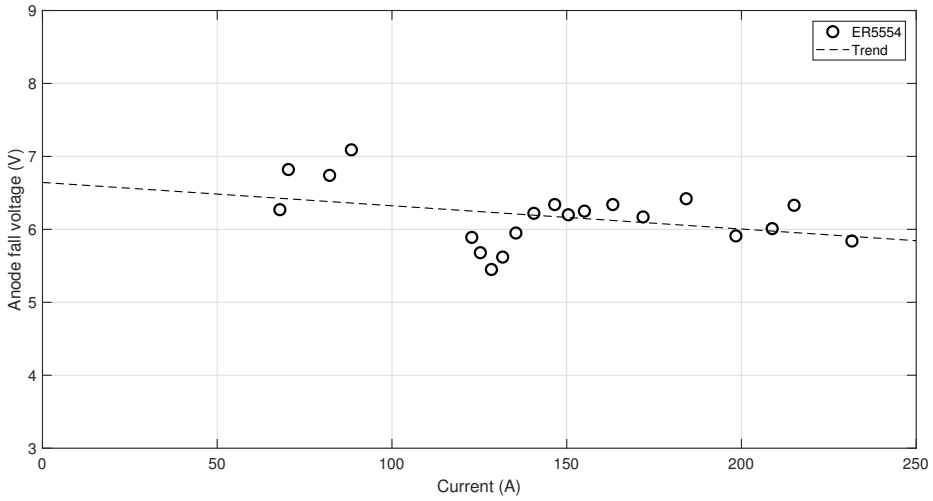

Figure 5.7: Anode fall voltage and current for ER5554.

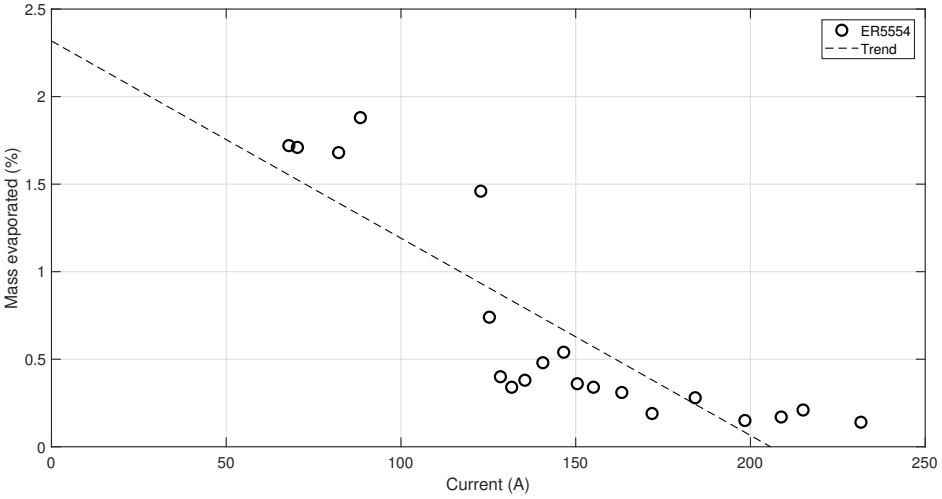

Figure 5.8: Evaporation percentage and current for ER5554.

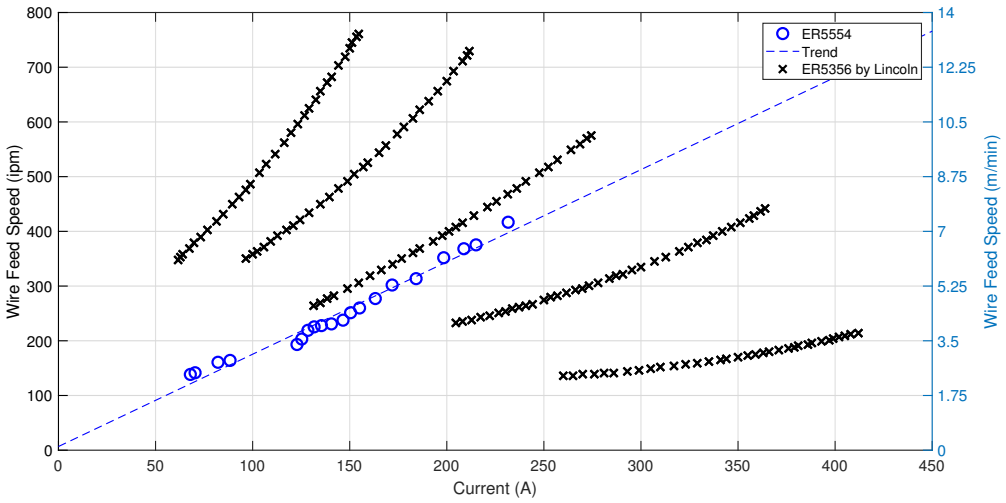

Figure 5.9: Wire feed speed and current for ER5554.

5.0.1.4. ER5183

For the electrode ER5183 the data is shown in Table 5.4. This table contains for every current measured the results for the anode fall voltage, the heat on the anode, the mass evaporated and the rate between the anode fall voltage and the total voltage of the measurement.

Table 5.4: General results for ER5183.

I A	V_{anode} V	Q_{anode} W	Evap. %	$V_{\text{anode}}/V_{\text{total}}$ %
61,81	6,88	425,13	1,17%	29,52%
69,55	6,56	456,14	0,88%	28,78%
82,16	6,72	552,05	0,37%	28,24%
99,27	5,66	561,76	0,22%	23,50%
111,72	5,86	655,03	0,21%	23,99%
126,45	5,14	649,95	0,14%	20,45%
129,69	5,22	677,05	0,11%	20,63%
137,07	5,42	743,35	0,10%	20,96%
139,36	6,08	847,07	0,11%	23,34%
146,53	6,35	931,06	0,09%	23,96%
155,66	6,59	1026,52	0,13%	24,66%
160,92	7,05	1133,90	0,09%	25,53%
172,73	7,02	1212,03	0,06%	24,69%
185,83	7,22	1341,11	0,05%	24,95%
211,70	6,36	1346,60	0,04%	22,09%
224,58	6,28	1409,66	0,04%	21,46%

When the above data is plotted, the following two figures can be obtained.

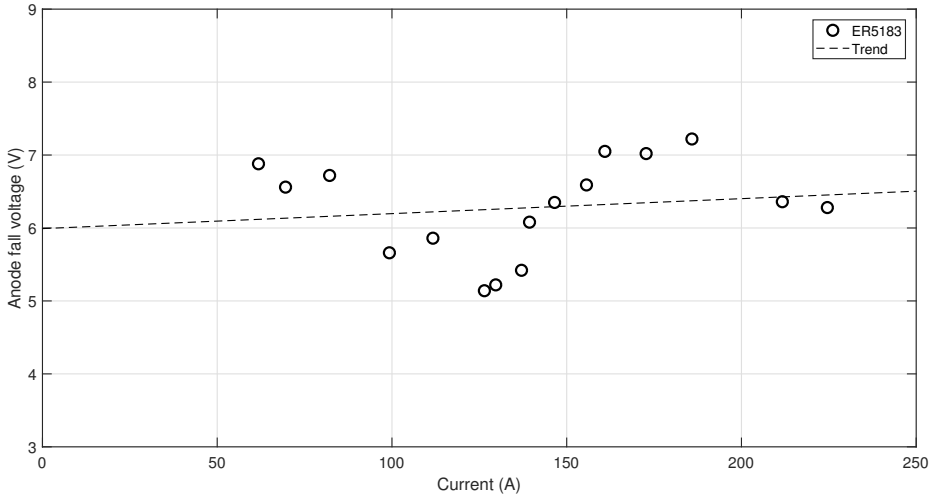

Figure 5.10: Anode fall voltage and current for ER5183.

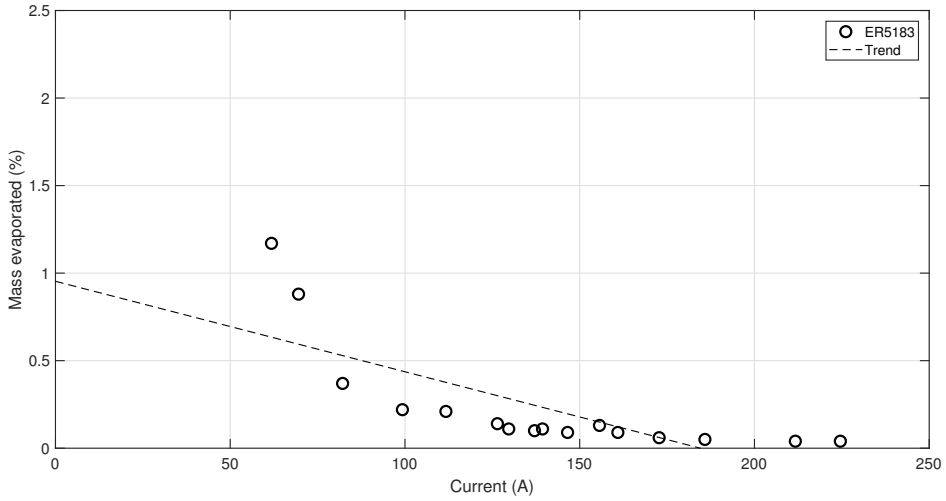

Figure 5.11: Evaporation percentage and current for ER5183.

From Equation 4.22 it is possible to plot the WFS and the current to compare it with the recommendation given by the Lincoln GMAW Brochure.

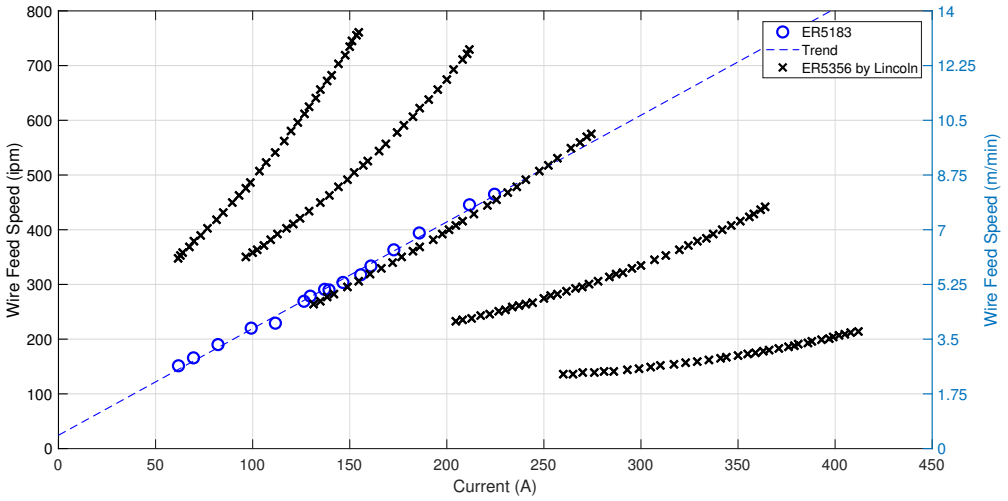

Figure 5.12: Wire feed speed and current for ER5183.

5.0.1.5. ER80SG

For the electrode ER80SG the data is shown in Table 5.5. This table contains for every current measured the results for the anode fall voltage, the heat on the anode, the mass evaporated and the rate between the anode fall voltage and the total voltage of the measurement.

Table 5.5: General results for ER80SG.

I A	V_{anode} V	Q_{anode} W	Evap. %	$V_{\text{anode}}/V_{\text{total}}$ %
136,28	4,71	641,27	0,23%	16,16%
144,41	4,49	648,75	0,23%	15,17%
147,97	6,08	899,35	0,29%	20,77%
155,07	4,83	749,71	0,34%	16,61%
161,13	4,26	686,03	0,46%	14,67%
180,84	4,37	789,76	0,42%	15,52%
191,41	4,14	792,20	0,32%	14,10%
198,83	4,18	831,04	0,02%	14,36%
199,62	4,11	820,78	0,24%	14,31%
212,23	4,83	1025,83	0,31%	16,15%
231,28	4,65	1075,80	0,29%	15,46%
241,25	4,96	1196,43	0,39%	16,49%
259,46	5,00	1296,68	0,38%	16,32%
314,90	5,20	1637,84	0,45%	16,04%
328,56	5,58	1831,99	0,43%	17,01%

When the above data is plotted, the following two figures can be obtained.

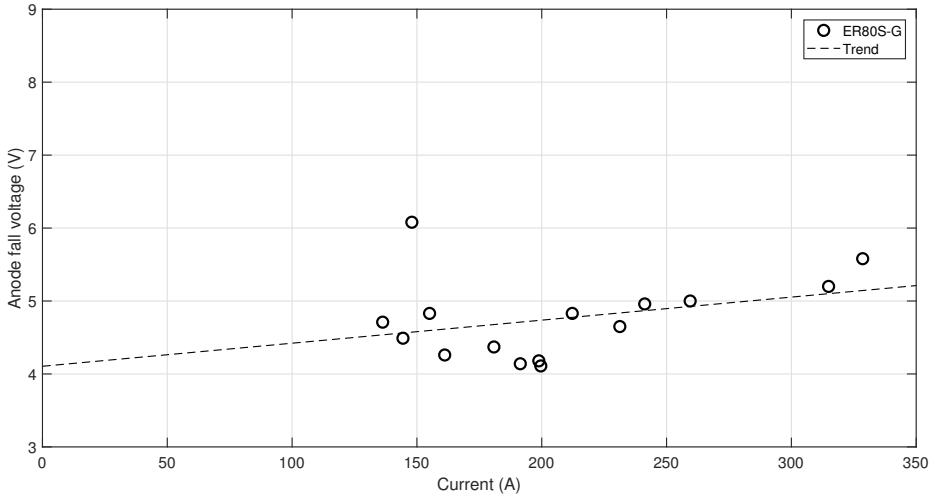

Figure 5.13: Anode fall voltage and current for ER80SG.

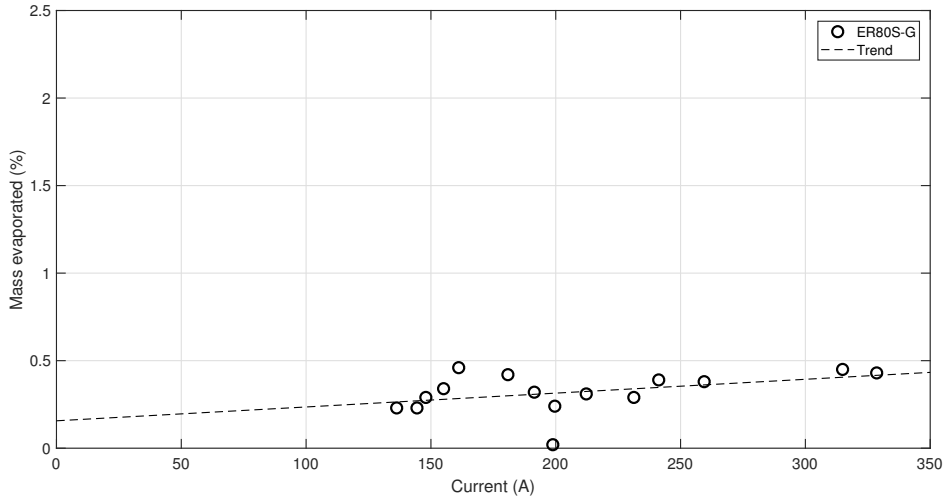

Figure 5.14: Evaporation percentage and current for ER80SG.

From Equation 4.22 it is possible to plot the WFS and the current to compare it with the recommendation given by the Lincoln GMAW Brochure.

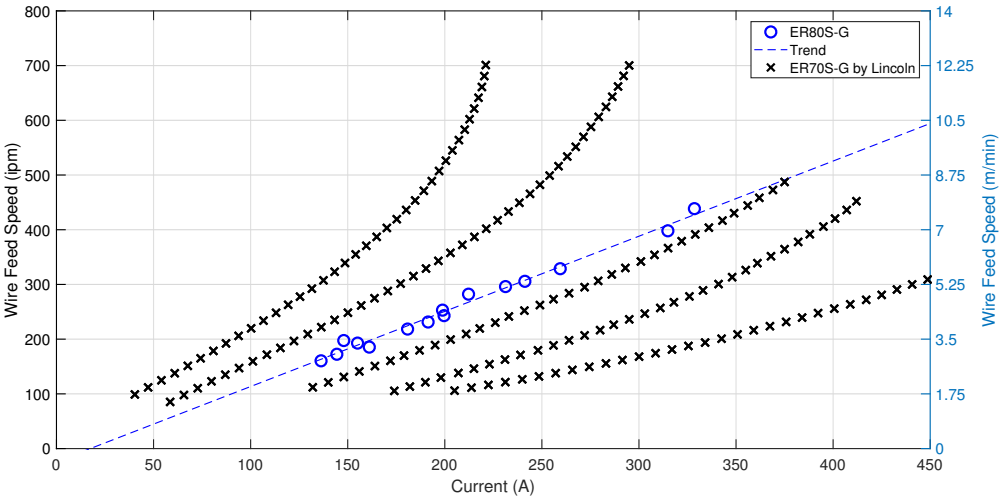

Figure 5.15: Wire feed speed and current for ER80SG.

5.0.1.6. Pure Fe

For the electrode pure Fe the data is shown in Table 5.6. This table contains for every current measured the results for the anode fall voltage, the heat on the anode, the mass evaporated and the rate between the anode fall voltage and the total voltage of the measurement.

Table 5.6: General results for pure Fe.

I A	V_{anode} V	Q_{anode} W	Evap. %	$V_{\text{anode}}/V_{\text{total}}$ %
116,23	3,09	358,91	0,33%	11,26%
144,10	3,32	478,55	1,08%	11,53%
171,45	3,84	658,08	1,62%	13,20%
177,96	4,06	723,11	1,81%	13,89%
183,76	3,93	721,94	1,38%	13,24%
191,84	3,66	701,34	0,94%	12,40%
197,02	3,63	714,78	0,78%	12,23%
217,75	3,84	836,07	1,26%	12,95%
222,37	4,55	1012,00	2,25%	15,25%
222,43	4,98	1107,60	2,20%	16,44%
237,92	4,27	1015,22	1,42%	14,20%
271,79	4,55	1235,57	1,56%	14,88%
272,66	4,98	1357,04	1,67%	15,77%

When the above data is plotted, the following two figures can be obtained.

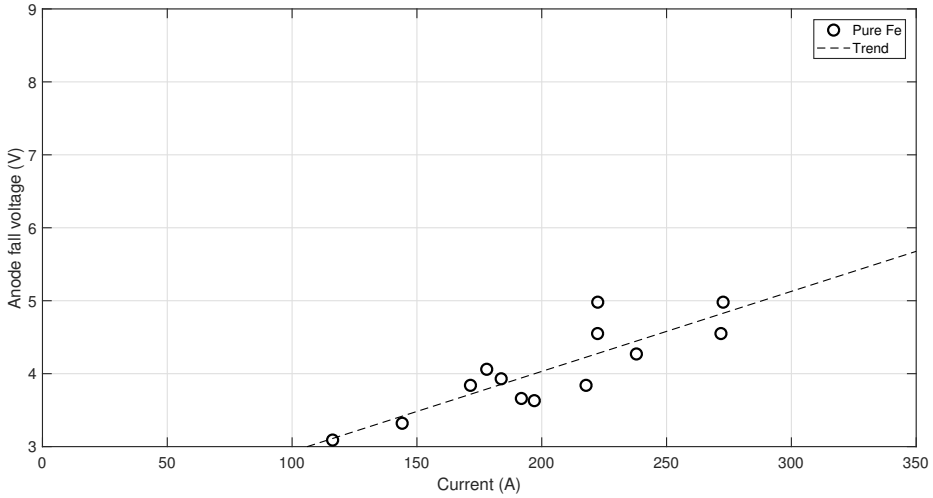

Figure 5.16: Anode fall voltage and current for pure Fe.

From Equation 4.22 it is possible to plot the WFS and the current to compare it with the recommendation given by the Lincoln GMAW Brochure.

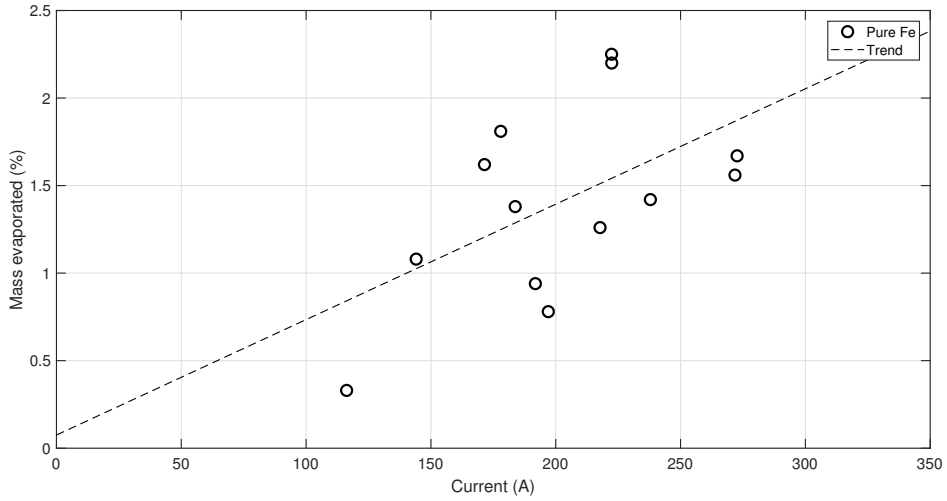

Figure 5.17: Evaporation percentage and current for pure Fe.

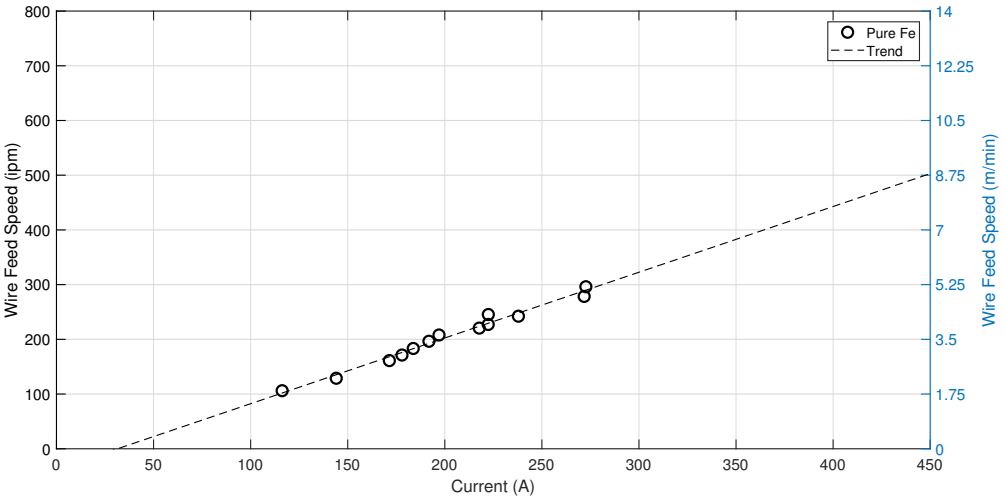

Figure 5.18: Wire feed speed and current for pure Fe.

5.0.1.7. Voltages comparison

When analysing all the electrodes together, the following graph is obtained for anode fall voltages.

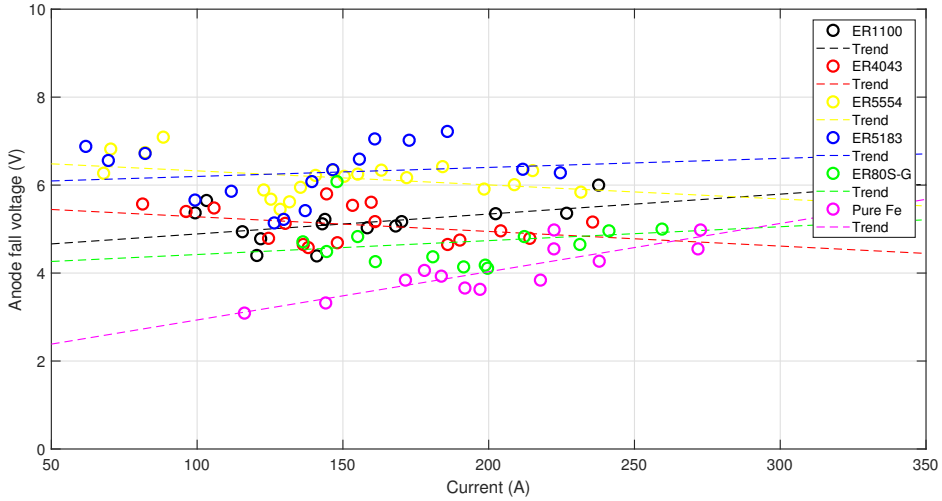

Figure 5.19: Anode fall voltage and current for every measurement.

With all the data shown in the graphics above, the values of voltages at 200 (A), the slopes of the trend lines, transition currents by Lowke [11] and the transition currents out of the videos were obtained and compared in Table 5.7.

Table 5.7: Anode fall voltage, slopes and transition currents by composite.

	V_{anode}^{200A} V	Slope V/A	I_{tran} (Lowke) A	I_{tran} (Videos) A
ER1100	5,333	0,005	170	200
ER4043	4,899	-0,003	174	200
ER5554	5,925	-0,003	166	230
ER5183	6,748	0,002	175	220
ER80SG	4,133	0,003	251	220
Pure Fe	3,658	0,011	261	-

With this data it is possible to write the following linear expressions for the anode fall voltage.

$$V_{\text{ER1100}} = 0,005I + 4,437 \tag{5.1}$$
$$V_{\text{ER4043}} = -0,003I + 5,617 \tag{5.2}$$
$$V_{\text{ER5554}} = -0,003I + 6,640 \tag{5.3}$$
$$V_{\text{ER5183}} = 0,002I + 5,992 \tag{5.4}$$
$$V_{\text{ER80SG}} = 0,003I + 4,106 \tag{5.5}$$
$$V_{\text{Pure Fe}} = 0,011I + 1,838 \tag{5.6}$$

5.1. Droplet evaporation comparison

When analysing all the electrodes together, the following figure is obtained for mass evaporated.

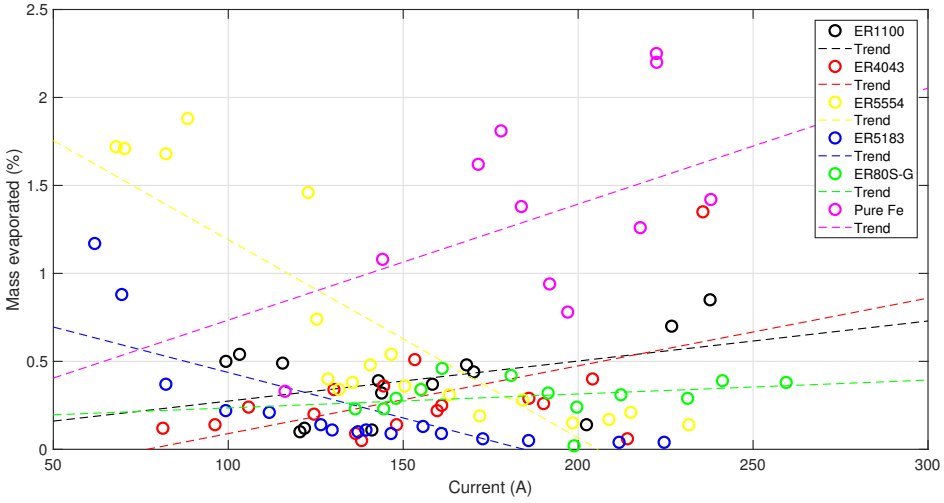

Figure 5.20: Evaporation percentage and current for every electrode.

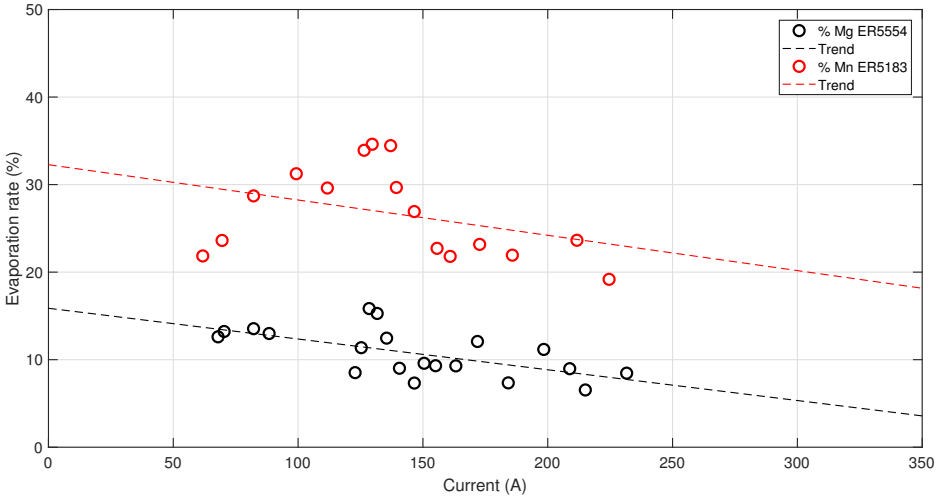

Figure 5.21: Evaporation percentage of Magnesium and Manganese.

5.2. Other measurements results

5.2.1. ER70S-G by Scott

For the electrode ER70SG the data is shown in Table 5.8. This table contains for every current measured the results for the anode fall voltage, the heat on the anode and the mass evaporated..

Table 5.8: General results for ER70SG by Scott.

I A	V_{anode} V	Q_{anode} W	Evap. %
181,1	3,232	585,2	0,020%
188,1	3,624	681,8	0,021%
188,7	3,787	714,8	0,021%
195,9	3,853	754,7	0,021%
197,8	3,651	722,4	0,021%
205,0	3,624	742,8	0,021%
206,9	3,820	790,2	0,021%
208,1	4,119	857,3	0,022%
215,3	3,943	848,9	0,021%
217,8	4,440	966,8	0,023%
228,1	4,457	1016,7	0,023%
232,0	4,488	1041,2	0,023%
234,6	4,422	1037,5	0,022%

When the above data is plotted, the following two figures can be obtained.

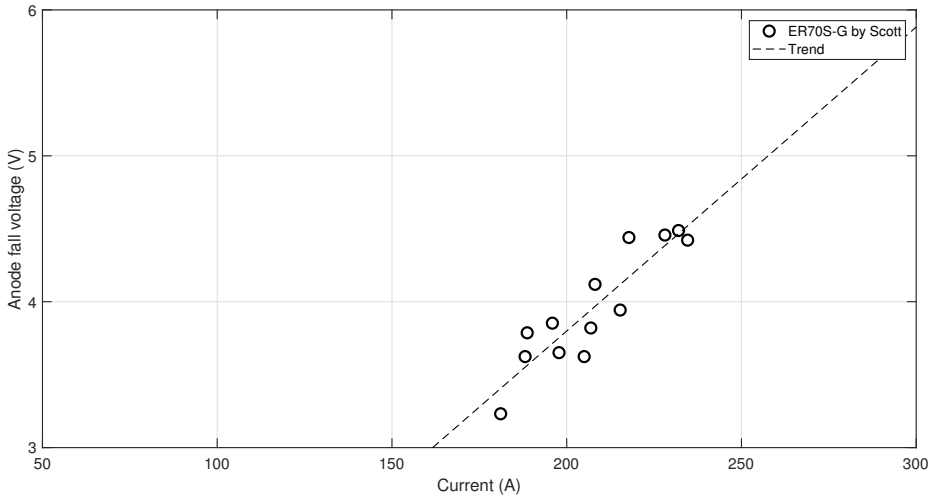

Figure 5.22: Anode fall voltage and current for ER70SG by Scott.

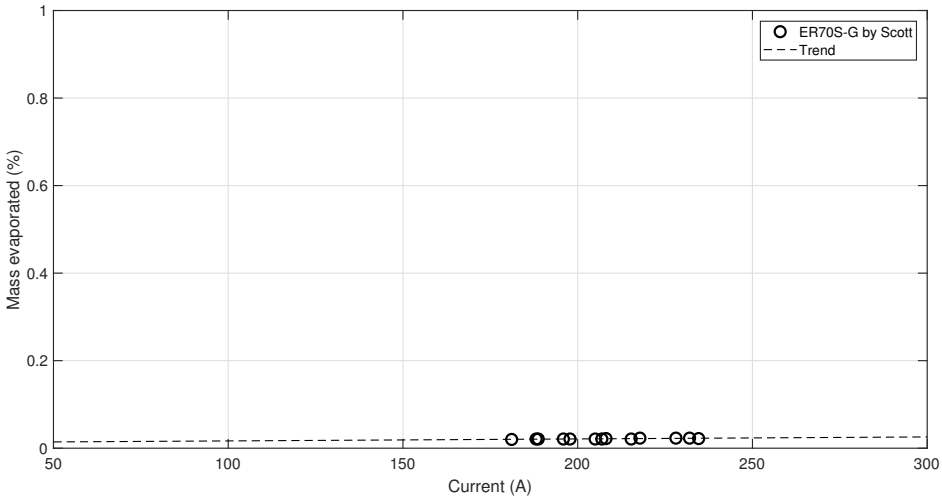

Figure 5.23: Evaporation percentage and current for ER70SG by Scott.

5.2.2. ER70SG by Soderstrom

For the electrode ER70SG the data is shown in Table 5.9. This table contains for every current measured the results for the anode fall voltage, the heat on the anode and the mass evaporated..

Table 5.9: General results for ER70SG by Soderstrom.

I A	V_{anode} V	Q_{anode} W	Evap. %
185,1	2,634	487,6	0,034%
186,1	3,084	573,8	0,019%
189,1	3,869	731,6	0,021%
197,1	3,845	757,9	0,021%
202,1	3,274	661,8	0,020%
204,2	2,494	509,3	0,023%
210,1	3,228	678,2	0,019%
214,1	3,680	787,7	0,021%
217,2	3,727	809,6	0,021%
227,2	3,906	887,7	0,021%
230,0	3,618	832,1	0,020%
247,9	4,479	1110,3	0,022%
251,2	4,200	1055,0	0,021%
255,0	4,160	1060,7	0,021%
257,2	4,782	1230,1	0,023%
261,1	4,389	1145,9	0,022%

When the above data is plotted, the following two figures can be obtained.

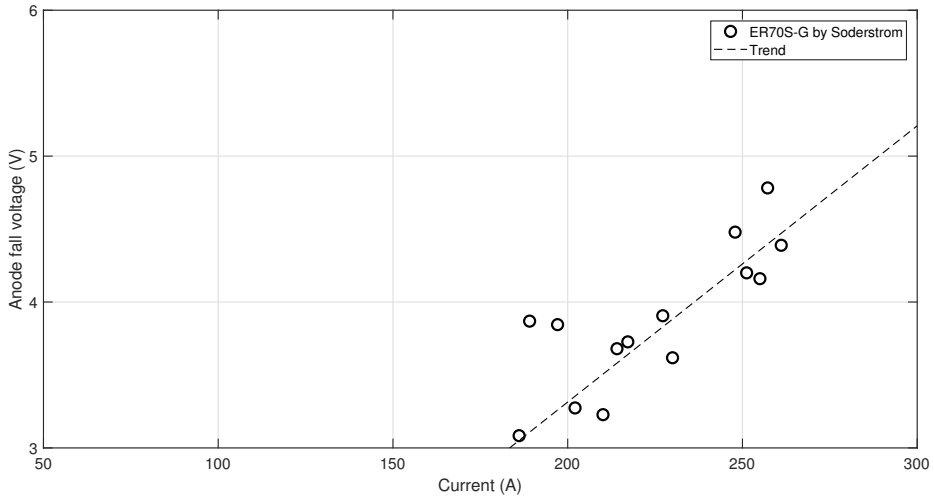

Figure 5.24: Anode fall voltage and current for ER70SG by Soderstrom.

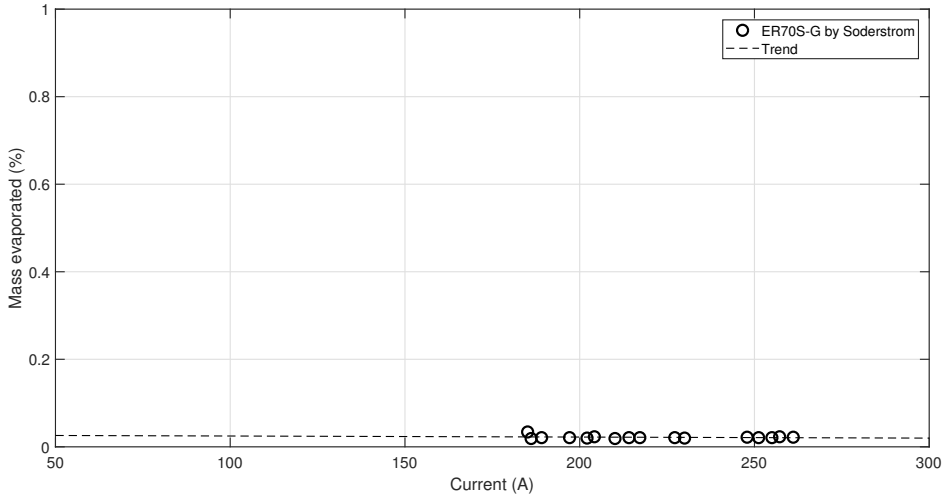

Figure 5.25: Evaporation percentage and current for ER70SG by Soderstrom.

5.2.3. ER4043 by Soderstrom

For the electrode ER4043 the data is shown in Table 5.10. This table contains for every current measured the results for the anode fall voltage, the heat on the anode and the mass evaporated..

When the above data is plotted, the following two figures can be obtained.

Table 5.10: General results for ER4043 by Soderstrom.

I A	V_{anode} V	Q_{anode} W	Evap. %
85	4,007	339,5	0,090%
100	3,912	391,7	0,107%
107	3,878	414,3	0,123%
118	3,767	443,7	0,143%
134	3,563	477,2	0,166%
146	3,458	504,3	0,192%
149	3,476	517,2	0,222%
165	3,423	564,7	0,257%
170	3,459	587,8	0,297%
181	3,493	632,6	0,343%
195	3,540	691,2	0,395%
221	3,596	795,0	0,451%

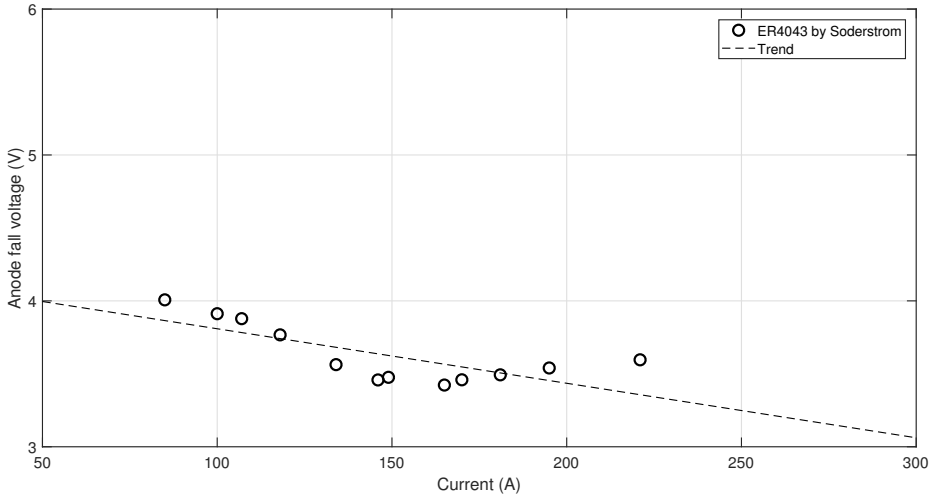

Figure 5.26: Anode fall voltage and current for 4043 by Soderstrom.

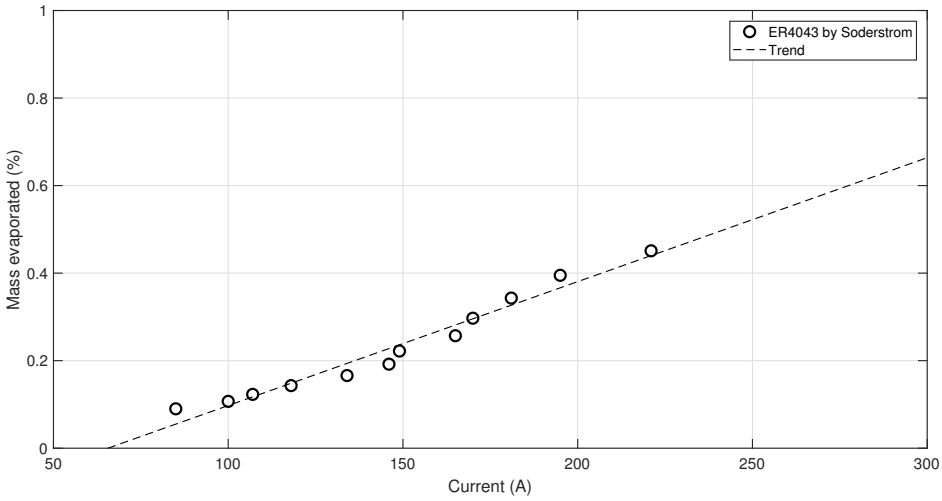

Figure 5.27: Evaporation percentage and current for ER4043 by Soderstrom.

Chapter 6

Discussion

6.1. Anode fall voltage

The first point to analyse is the behaviour of the values for the different anode fall voltages of the electrodes. In almost all cases, the anode fall voltage tends to increase with the current. The different slopes of the trending lines are shown in Table 5.7, where it is possible to see that it increases very little or decreases in two cases, but still with a slope smaller than $0,005 V/A$. It can be seen that the trend line of every electrode does not fit perfectly, as it is possible to see a minimum value on the middle of the X axis, between 100 and 200 A in all cases but the one of pure iron.

This small decrease on the anode fall voltage is always close to the current transition, as it can be seen on Table 5.7. Due to the amount of videos, in cannot be seen exactly, but based on Lowkes work it is possible to see an approximation. This small decrease of anode fall voltage behaves like the droplet temperature in the transition current, as by McIntosh *et al.* [24]. This decrease on voltage could be because of two reasons: temperature drop and less evaporation. In some cases can be seen that the evaporation has a minimum close to the transition current. When analysing Equation 4.27, the two items are the ones that could make the anode fall voltage decrease.

When obtaining the anode fall voltage for 200 A it is possible to see that they do not change considerably. Between 7 and 3,5 V for all the electrodes. It is possible to see on every table for electrodes, what amount of potential loss was consumed by the anode, in comparison with the total voltage of the process. This value changes considerably when changing from electrode. For both electrodes out of steel it behaves close to a 15% of the total voltage. In the case of aluminium electrodes it varies between 20% for ER1100 and ER4043, but for ER5554 and ER5183 above 20% almost in every measurement. This energy consumption linked close to the electrode, is related on the composition of them. The ER5XXX electrodes contain big amounts of manganese and magnesium.

In Figure 5.19 is possible to see the comparison between all electrodes. It is interesting to see how the majority of the results stay between 4 and 6 V. It is possible to say that a value of 5 V is possible to use as an approximation, but always considering that it could change according to the electrode composition and current. As seen in the figures, it is difficult to say that the anode fall voltage is independent of every current value, but due to the relatively flat slope of the trending lines is possible to use it constant as an approximation.

6.2. Mass evaporated

The percentage of mass evaporated changes according to different variables, but two crucial ones are the droplet temperature and the electrode composition. The transfer mode varies with the current, being globular with low currents and spray with higher ones. Close to the transition current there is no distinct behaviour of the mass evaporated. The mass evaporated has tends to increase with the current, as also with increasing temperature. As the temperature increases, it is expected for the droplet to evaporate more mass. As equations are made following a quasi steady state, it is not expected to have less evaporation on the droplet when increasing the current, and so the frequency of detachment, as this calculations were made over time.

When analysing the different compositions of the electrodes is important to study the ER5XXX electrodes, as those are the ones that have high amounts of magnesium and manganese on them. This two elements have low boiling temperatures, being sometimes lower than the droplet temperature on some measurements. This means that when these elements start to boil, the droplet looses energy on giving heat to these elements that are boiling, what affects directly to the droplet temperature. As the droplet does not increases its heat drastically, the Mn and Mg boils and it goes out of the control volume as mass evaporated. It is important to acknowledge, that when Mn and Mg are present on the electrode, they evaporate in big amounts as can be seen in Figure 5.21. This big amounts of evaporation, as it occurs very fast, create high amounts of sparks on the process. This mass that goes out of the control volume, also affects the general power generated on the droplet, as it goes hot mass out and decreases the average temperature of the droplet.

A third point that also affects drastically on the evaporation is the surface area of the droplet. When the transfer mode is globular, the droplets are bigger than the electrode diameter. The evaporation is calculated over surface and when there is more surface over the same evaporation rate, there is more evaporation. When the transfer mode is clearly on spray transfer, the droplet does not creates a spherical geometry, as it could also be smaller than the electrode diameter. This proves that the calculation is not completely accurate, because the area is just assumed to be a sphere. This calculation of the area is made empirically, by using the frequency of detachment of the droplet out of the videos recorded. This is why the amount of evaporation is higher with globular transfer than with spray transfer, as the area of the droplet is directly dependant on this parameter. As it is one parameter that affects on a big scale the evaporation, it should be revisited on future works.

When comparing the anode fall voltage and the mass evaporated, it is interesting how the behaviours of them can be related to the electrode composition. In the first case, it is clear how the droplet temperature affects the anode fall voltage and the mass evaporated. As the ER1100 electrode is almost pure aluminium, as the current increases also does the droplet temperature. With those two variables increasing, the anode fall voltage and the evaporation also increases. The same behaviour can be seen on steel electrodes ER80S-G and pure Fe. In the case of the ER4043, the anode fall voltage has a small tendency to decrease, but it is always near the 5 V. In this case the evaporation does increases, but not drastically. This electrode behaves very stable, with the anode fall voltage decreasing and the evaporation increasing. This is given by the different elements that has on its composition: Si, Fe and Cu. These three elements have a high boiling temperature and also higher specific heats than aluminium, properties that make the evaporation to behave stable.

When analysing Figure 5.20 is possible to notice how the evaporation always increases with current. This is mainly given by the droplet temperature: as the temperature increases, also does the evaporation. This is when analysing the general and not by droplet that falls. It is clear that every material behaves different. All the differences are because of the composition, as they are on a same range of current. For electrodes ER1100 (close to pure Al) and pure Fe it is interesting to see their linear behaviour. It is important to remember that the frequency for pure iron was always 30 Hz and this could cause different behaviours. When adding different alloys, the curve tends to go up or down, depending on the alloys, which is mainly attributed to their Mn and Mg contents. The ER5XXX electrodes have more evaporation and it is mainly because of the Mn and Mg on their composition. It is possible to see on Figure 5.21 that a big amount of the mass evaporated is made out of this elements. The percentages show that a big amount of the total mass of Mn or Mg of the electrode is evaporated.

When looking at the rates of evaporation, it can be seen that the amount of mass evaporated in ER5554 or ER5183 electrodes is important. In the fifth value of Table 5.4 the evaporation is 0,22% and 30% of it is manganese. This evaporation occurs with a velocity higher than 3,5 mg/min that in the end would be almost 11 mg/min of Mn. In just a work hour of welding, out of the droplet is going to evaporate 66 mg that the welder could breathe. The National Institute for Occupational Safety and Health (NIOSH) limits the short term exposure limit in 3 mg/m^3 as a recommendation. This value in a small room without ventilation could easily be reached with the values previously noted. To prevent this evaporations on the droplet, the main goal is to have lower droplet temperatures, by for example working on the transition currents.

6.3. Wire Feed Speed

A very important point to analyse are the curves of the WFS per component. These curves are always given the the machine supplier on their brochure as a recommendation to use, being these ones from Lincoln Electric. For the calculations the WFS of the process is used for $\dot{m}_c$, but for the calculation of the anode fall voltage. This WFS gives in all electrodes the same behaviour as the ones given by Lincoln Electric on its brochure, always ascending

when the current increases. This behaviour is a very good approach, because it gives the point that the model generated is good and behaves according to what is expected for the machine to work.

When analysing the values of the curves the calculations are very close to what is expected from the machine. The difference is marginal and it is according to the electrode diameter. Some calculations are not easy to compare with the curves, because it does not work with the full range of currents or electrode composition, but it can be seen that the behaviours are according to the curves. It is an unknown how these curves are being made by the supplier, as they can consider more variables that these models do not. The WFS can affect on the heat from the weld, considering here the cathode or other variables that are not considered in this model.

6.4. Comparison

When analysing different measurements under the model generated, it is possible to see that the behaviour of the results are according to the results obtained from the data studied. The first to analyse is the ER4043 by Soderstrom, because it can be compared with the one measured. It is possible to see on Figure 5.26 that the tendency of the curve is going down. The slow decrease of anode fall voltage is very similar to the one on Figure 5.4. It is also possible to see a minimum between 120 and 200 A, that is where the transition current is found for this electrode. This minimum has to correspond to the minimum temperature. With that in mind it is possible to understand the influence of the droplet temperature on the anode fall voltage. The mass evaporated behaves also in an increasing way, just how the results obtained previously show on Figure 5.5, it increases with the current. In the results from Soderstrom measurements, it is possible to see that the percentage of evaporation is less than the previous one. It is important to acknowledge that the frequency used for Soderstrom is 30 Hz. This is used for all currents and is a value that can explain the evaporation rates. As the wire feed speed increases, the detachment frequency stays constant and the droplet diameter increases. To obtain more accurate values the frequencies of detachment should be obtained for every current.

The ER70S-G electrodes can be compared with the ER80S-G because of the proximity in composition, but should not give the same results. It can be seen that the three anode fall voltages increase with the current, but they are on different scales of every figure. When analysing Figures 5.22 and 5.24, both curves stay close to 4 V for currents between 150 and 250 A, what happens also with the measurements from Soderstrom. In Figure 5.13 between 150 and 200 A the anode fall voltage stays close to the 4 V. This small difference can be explained because of the difference in composition. As the ER70S-G has more Si, this one never evaporates and has a big specific heat. This difference can make the droplet temperature a bit cooler than the ER80S-G. When the data is studied, it can be seen that it has less droplet temperature the ER70S-G electrode for the same current. This difference in temperature affects on the mass evaporated too and as can be seen, the ER70S-G has less mass evaporated.

6.5. Observations

During the generation of the model, there were some considerations that needed to be done to complete it. The first consideration that needs to be commented on is that there are no heat losses because of radiation. These heat losses could occur on the droplet that is melted or on the electrode extension that is being heated because of the droplet. Following the Stefan-Boltzmann equation for black bodies, the heat lost by radiation for a droplet at 2500 °C would be less than 0,2 W for aluminium, that compared to the 1400 W of the process is insignificant. Another small consideration that could be added is the heat entering the system with the mass of the argon, as it enters the system at room temperature.

One last but not less important consideration made, is due to the calculation of the area of the droplet. First is that the droplet was considered to be a sphere in all cases, including spray transfer. In the videos, it can be seen that the welded metal is not just the droplet as a sphere, but also a small part of the electrode. This welded electrode that does not detach with a droplet is partially considered in the resistivity calculations. When obtaining the diameter of the droplet, it is made in an empirical way, considering the mass of the electrode entering the system and the one leaving with a frequency. This approximation was considering the frequency of detachment out of the videos made for the data acquisition. As the Equation 4.44 yielded droplet diameters that were not realistic, therefore, it was not considered.

Chapter 7

Conclusions

The model developed is a very good approach to understand the anode fall voltage and the mass evaporation on the droplet. These two topics, are still being studied theoretically and experimentally. The trending lines obtained are very useful to understand the behaviour of the anode fall voltage. A value of 5 V can be used for different approximations on works over aluminium or steel electrodes, but always remembering that a change of current or electrode composition can lead to voltage changes. The evaporation composition is also very useful for the industry, as with it could be possible to analyse what would be the composition of the droplet when it falls into the work piece. When working over new electrodes, the anode fall voltage and droplet composition are possible to know before doing the weld.

With all the work done here, it is possible to understand the consequences of a high droplet temperature. The first impact would be on the evaporation and then the anode fall voltage, that leads to higher energy consumptions. The behaviour of the droplet temperature is an important point for the manufacturers, because it is what needs to be understood to control and reduce evaporation on the droplet. The main variables to understand the anode fall voltage are the droplet temperatures, droplet evaporation and current.

The work here presented contains most of the theory behind the droplet evaporation as an approach to make it applicable. The behaviour of the droplet temperature and mass evaporated needs to be studied further, so that the different results can be applied to the design of new machines or materials in the future.

7.1. Future work

- Analyse the droplet geometry for every transfer mode.
- Study the current density of the measurements.
- Generate an energy balance inside the droplet.
- Compare with pulsed currents publications.
- Make new measurements for different parameters.

Bibliography

[1] D. H. Phillips, *Arc Welding Processes*, ch. 2, pp. 4–73. John Wiley and Sons, Ltd, 2016.

[2] C. McIntosh and P. F. Mendez, "Experimental Measurements of Fall Voltages in Gas Metal Arc Welding," *Welding Journal*, vol. Vol. 96, 2017.

[3] A. G. Y. Cressault, "Calculation of diffusion coefficients in air-metal thermal plasmas," *Journal of Physics D Applied Physics*, vol. 43, no. 43, 2010.

[4] C. McIntosh and P. F. Mendez, "Fall Voltages in Advanced Waveform Aluminum GMAW," *Welding Journal*, vol. 96, September 2017.

[5] G. Zhang, G. Gött, and D. Uhrlandt, "Study of the anode energy in gas metal arc welding," 2020.

[6] G. Zhang, G. Gött, R. Kozakov, D. Uhrlandt, U. Reisgen, K. Willms, R. Sharma, S. Mann, and P. Lozano Torrado, "Study of the wire resistance in gas metal arc welding," *Journal of Physics D Applied Physics*, vol. 52, 12 2018.

[7] Wikipedia, "Gas metal arc welding," Visited: 2021.

[8] J. Lancaster, *The physics of Welding*. Pergamon international library of science, technology, engineering, and social studies, Cambridge: Oxford: Pergamon, 1984.

[9] J. Metcalfe and M. Quigley, "Heat Transfer in Plasma-Arc Welding.," *Welding Research Abroad*, pp. 99–104, 1975.

[10] J. D. Kraus and K. R. Carver, "Electromagnetics," 1973.

[11] J. Lowke, "Globular and Spray Transfer in MIG Welding," *Weld World*, vol. 55, pp. 19–23, 2011.

[12] P. Mendez, "Voltage in Arc Welding," (University of Alberta, Edmonton), 2020.

[13] D. T. S.-H. M. B. C. Quigley, P. H. Richards and A. E. F. Gick, "Heat flow to the workpiece from a TIG welding arc," *Journal of Physics D: Applied Physics*, vol. 6, no. 18, p. 2250–2258, 1973.

[14] G. R. Lehnhoff and P. F. Mendez, "Scaling of non-linear effects in heat transfer of a continuously fed melting wire," *International Journal of Heat and Mass Transfer*, vol. 95, no. 54, pp. 2651—2660, 2011.

[15] I. Langmuir, "The vapor pressure of metallic tungsten," *Phys. Rev.*, vol. 2, pp. 329–342, Nov 1913.

[16] V. P. I. C. B. Alcock and M. K. Horrigan, "Vapour Pressure Equations for the Metallic Elements: 298-2500 K," *Canadian Metallurgical Quarterly*, vol. 23, no. 3, pp. 309–313, 1984.

[17] "CRC Handbook of Chemistry and Physics, 84th Edition Edited by David R. Lide.," *Journal of the American Chemical Society*, vol. 126, no. 5, 2004.

[18] M. A. R. P. F. Mendez, T. W. Eagar and G. Trapaga, "Order-of-magnitude scaling of the cathode region in an axisymmetric transferred electric arc," *Metallurgical and Materials Transactions B*, vol. 32, pp. 547–554, 2001.

[19] E. J. Soderstrom, *Gas Metal Arc-Welding Electrode Heat-and-Mass Transfer Mechanisms*. Doctor of philosophy, Colorado School of Mines, 2009.

[20] D. R. Poirier and G. H. Geiger, *Fick's Law and Diffusivity of Materials*, pp. 419–461. Cham: Springer International Publishing, 2016.

[21] J. M. P. R. C. Reid and T. K. Sherwood, *The Properties of Gases and Liquids*, pp. 549–550. McGraw-Hill, 1977.

[22] E. T. Turkdogan, P. Grieveson, and L. S. Darken, "Enhancement of diffusion-limited rates of vaporization of metals," *The Journal of Physical Chemistry*, vol. 67, no. 8, pp. 1647–1654, 1963.

[23] K. M. Scott, *Heat Transfer and Calorimetry of Tubular Ni/WC Wires Deposited with GMAW*. Master of science, University of Alberta, Edmonton, Canada, 2011.

[24] C. Mcintosh, J. Chapuis, and P. Mendez, "Effect of Ar-CO2 Gas Blends on Droplet Temperature in GMAW," vol. 95, pp. 273s–279s, 08 2016.

Appendant A

Data used

The following tables show the initial data given by the measurements performed by Zhao Yang.

Table A.1: Initial data used for a 1,2 mm ER1100 electrode.

I A	WFS inch/min	U_c m/s	T_0 °C	T_d °C	q_c W
99,32	160	0,072	20	2235,6	875,4
103,22	170	0,076	20	2322	918,23
115,52	170	0,076	20	2359	1039,7
120,48	180	0,080	20	2109,1	1128,1
121,79	190	0,085	20	2180,5	1012,4
141,04	200	0,089	20	2217,1	1018,6
142,9	210	0,093	20	2460,3	1238,9
143,83	220	0,098	20	2419,9	1209,7
158,35	230	0,102	20	2454,8	1579,9
168,1	240	0,106	20	2509,2	1324
170,15	250	0,110	20	2492,7	1625,3
202,38	300	0,131	20	2574,5	1796,7
226,73	350	0,152	20	2508,8	2303,1
237,71	400	0,171	20	2591,5	2752,7

Table A.2: Initial data used for a 1,2 mm ER4043 electrode.

I A	WFS inch/min	U_c m/s	T_0 °C	T_d °C	q_c W
81,3	135	0,060	20	1907,4	659,2
96,2	155	0,069	20	1934,9	861,5
105,8	165	0,074	20	2063,4	813,5
124,5	175	0,078	20	2096,7	999,9
130,2	185	0,083	20	2258,0	966,4
136,4	195	0,087	20	2045,4	1216,5
138,1	200	0,089	20	1985,8	1218,2
148,1	210	0,093	20	2174,6	1267,3
144,4	225	0,100	20	2366,0	535,1
153,3	230	0,102	20	2437,9	971,5
161	240	0,106	20	2345,5	1194,5
159,7	250	0,110	20	2373,6	1236,9
185,9	260	0,115	20	2477,2	1692,6
190,11	270	0,119	20	2505,2	1458,6
204,12	290	0,127	20	2639,0	1349,6
214,09	310	0,135	20	2538,2	1698,9
235,65	350	0,152	20	2662,9	1820,8

Table A.3: Initial data used for a 1,2 mm ER5554 electrode.

I A	WFS inch/min	U_c m/s	T_0 °C	T_d °C	q_c W
67,93	145	0,065	20	1605,7	555,7
70,37	155	0,069	20	1708,5	582,4
82,16	175	0,078	20	1768,4	694,1
88,39	185	0,083	20	1917,6	831,9
122,84	195	0,087	20	2208,8	1047,3
125,3	200	0,089	20	2125,2	1146,5
128,46	210	0,093	20	1987,5	1195,3
131,68	220	0,098	20	2013,2	1165,7
135,46	230	0,102	20	2108,8	1322,2
140,6	240	0,106	20	2210,5	1505,3
146,56	250	0,110	20	2268,9	1418,4
150,46	260	0,115	20	2196,2	1641,5
155,07	270	0,119	20	2205,7	1525,0
163,19	290	0,127	20	2207,1	1643,1
171,85	310	0,135	20	2133,6	1738,0
184,19	330	0,144	20	2273,1	1986,7
198,41	350	0,152	20	2161,5	2165,5
208,8	370	0,160	20	2223,1	2513,9
215,06	390	0,167	20	2305,4	2360,9
231,61	410	0,175	20	2240,3	2758,2

Table A.4: Initial data used for a 1,2 mm ER5183 electrode.

I A	WFS inch/min	U_c m/s	T_0 °C	T_d °C	q_c W
61,81	145	0,065	20	1594,6	617,7
69,55	155	0,069	20	1616,5	564,1
82,16	180	0,080	20	1720,8	725,9
99,27	190	0,085	20	1683,1	895,0
111,72	200	0,089	20	1909,3	914,1
126,45	220	0,098	20	1733,7	1289,5
129,69	230	0,102	20	1731,9	985,3
137,07	245	0,108	20	1803,0	1523,5
139,36	260	0,115	20	1948,1	1402,5
146,53	280	0,123	20	2005,2	1541,2
155,66	300	0,131	20	2085,7	1136,6
160,92	330	0,144	20	2105,3	1375,4
172,73	360	0,156	20	2087,2	1856,0
185,83	400	0,171	20	2109,3	1649,9
211,7	420	0,179	20	2086,7	2347,4
224,58	435	0,185	20	2157,2	2473,9

Table A.5: Initial data used for a 1,2 mm ER580S-G electrode.

I A	WFS inch/min	U_c m/s	T_0 °C	T_d °C	q_c W
136,28	150	0,0667245	20	2191,5	1718,2
144,41	160	0,0712028	20	2189,2	1954,9
147,97	190	0,0846293	20	2225,1	1866,6
155,07	180	0,0801552	20	2254,3	1846,7
161,13	170	0,0756797	20	2312,8	2039,8
180,84	200	0,089102	20	2313,2	1985,2
191,41	210	0,0935733	20	2280,5	2176,4
198,83	230	0,1025117	20	2255,4	2004,7
199,62	220	0,0980432	20	2279,9	2321,8
212,23	260	0,1159088	20	2335,7	2706,7
231,28	270	0,1203717	20	2361,3	2640,1
241,25	280	0,1248332	20	2441,2	2826,9
259,46	300	0,133752	20	2456,5	2652,9
314,9	360	0,1604748	20	2516,7	3819,5
328,56	400	0,178262	20	2527,7	4170,3

Table A.6: Initial data used for a 1,2 mm pure Fe electrode.

I A	WFS inch/min	U_c m/s	T_0 °C	T_d °C	q_c W
116,23	100	0,044	20	2095,6	1431,9
144,1	120	0,053	20	2293,5	2014,7
171,45	150	0,067	20	2376,9	2367,3
177,96	160	0,071	20	2401,5	2532,7
183,76	170	0,076	20	2351,5	2503,8
191,84	180	0,080	20	2280,7	2549,2
197,02	190	0,085	20	2251,7	2698,8
217,75	200	0,089	20	2338,7	2826,5
222,37	210	0,094	20	2455,4	2827,1
222,43	230	0,103	20	2458,2	3041,7
237,92	220	0,098	20	2459,3	2985,3
271,79	250	0,111	20	2547,5	3337,0
272,66	270	0,120	20	2565,6	3573,1

Appendant B

Composition

The composition of the different wires used are in the next tables and obtained from the Lincoln Brochure for GMAW.

Table B.1: Aluminium electrodes composition from Lincoln Brochure

AWS A5.10-92 Classification	%Mn	%Si	%Fe	%Mg	%Cr	%Cu	%Ti	%Zn	%Be	% others	%Al
ER4043	0,05	4,5-6,0	0,8	0,05	-	0,30	0,20	0,10	< 0,0008	0,05	Balance
ER1100	0,05	-	-	-	-	0,05-0,2	-	0,1	-	0,05	Balance
ER5554	0,5-1,0	0,25	0,4	2,4-3,0	0,05-0,2	0,1	0,05-0,2	0,25	< 0,0008	0,05	Balance
ER5183	0,5-1,0	0,4	0,4	4,3-5,2	0,05-0,25	0,1	0,15	0,25	< 0,0008	0,05	Balance

Table B.2: Steel electrodes composition from Lincoln Brochure

AWS A5.18 Classification	%C	%Mn	%Si	%S	%Ni	%Cr	%Mo	%Cu	%P	%Al	%V	%Zr+Ti
ER80S-G	0,08	1,4	0,08	<0,02	0,8	0,25	<0,05	<0,4	<0,02	<0,02	<0,03	<0,15
ER70S-G	0,05-0,15	0,8-1,4	0,3-0,6	<0,02	-	-	-	<0,02	<0,02	-	-	-
Pure Fe	<0,02	<0,2	-	<0,015	-	-	-	<0,06	<0,015	-	-	-

Appendant C

Enthalpies

The different enthalpies and temperatures are different in every material. The next figures show the relation between temperature and enthalpy for every material. All the data was obtained from JMatPro.

C.1. ER4043

Table C.1: Temperatures and enthalpies Al 4043

	Temperature K	Enthalpy kJ/kg	Specific heat J/kgK	Δi kJ/kg
T_0	293,15	-29,1	891,19	
T_{solidus}	853,15	738,9		5,33 10^2
T_{liquidus}	903	1050		5,33 10^2
$T_{\text{ref,l}}$	1773,15	2056,6	1159,1	
T_{boil}	2743,15	3181,1	1,05 10^6	
T_{g}	2743,15	4231,1		

The data above is shown in the next figure.

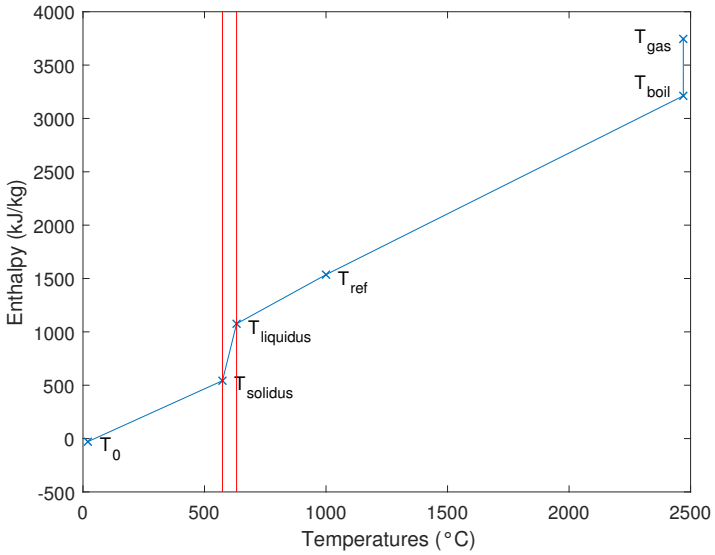

Figure C.1: Enthalpy and temperatures Al 4043.

C.2. ER1100

Table C.2: Temperature, enthalpies and specific heat for ER1100.

	Temperature K	Enthalpy kJ/kg	Specific heat (slope) J/kgK	Δi kJ/kg
T_0	20	-1,721	899,15	
T_{solidus}	933,15	1065,73		
T_{liquidus}	943,15	1077,46		
T_{ref}	1773,15	2052,49	1174,77	2,05 10^3
T_{boil}	2743,15	3192,0		
T_{g}	2743,15	4242,0		

The data above is shown in the next figure.

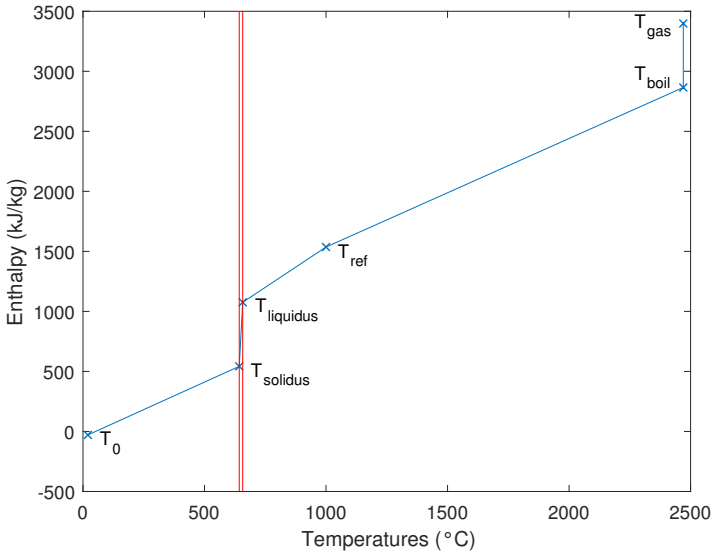

Figure C.2: Enthalpy and temperatures ER1100.

C.3. ER5554

Table C.3: Temperature, enthalpies and specific heat for ER5554.

	Temperature K	Enthalpy kJ/kg	Specific heat (slope) J/kgK	Δi kJ/kg
T_0	298,15	-39,002	8961,49	
T_{solidus}	874,48	583,18		4,99 10^2
T_{liquidus}	973,15	1081,87		
T_{ref}	1773,15	2021,11	1175,42	
T_{boil}	2743,15	3161,4		
T_{g}	2743,15	4211,4		1050

The data above is shown in the next figure.

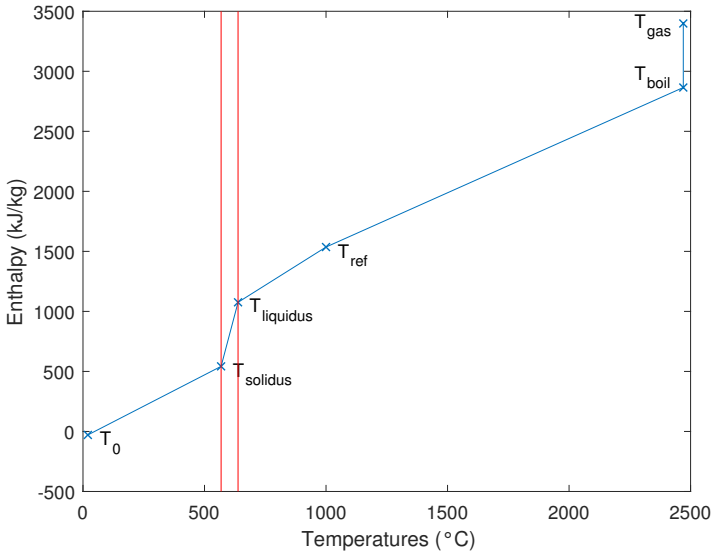

Figure C.3: Enthalpy and temperatures ER5554.

C.4. ER5183

Table C.4: Temperature, enthalpies and specific heat for ER5183.

	Temperature K	Enthalpy kJ/kg	Specific heat (slope) J/kgK	Δi kJ/kg
T_0	303,15	-39,75	902,49	
T_{solidus}	853,15	584,38		5,33 10^2
T_{liquidus}	1003,15	1112,89		5,33 10^2
T_{ref}	1773,15	2021,62	1174,77	
T_{boil}	2743,15	3168,0		
T_{g}	2743,15	4218	1050	

The data above is shown in the next figure.

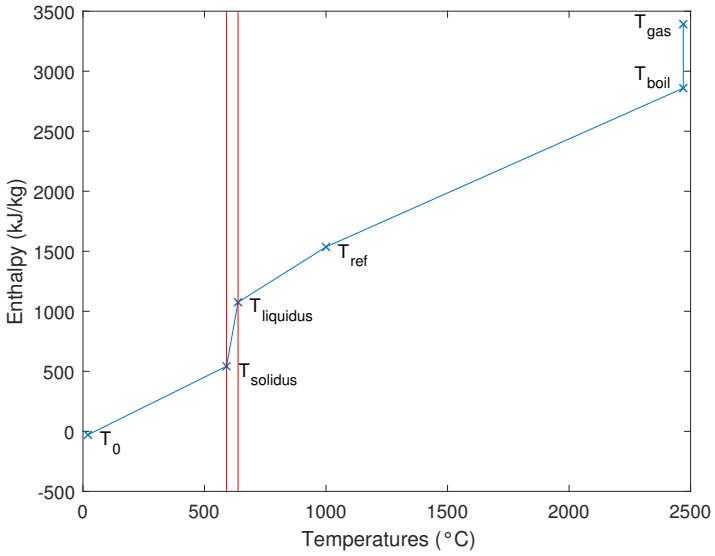

Figure C.4: Enthalpy and temperatures ER5183.

C.5. ER80S-G

Table C.5: Temperature, enthalpies and specific heat for ER80S-G.

	Temperature K	Enthalpy kJ/kg	Specific heat (slope) J/kgK	Δi kJ/kg
T_0	293,15	-19,05	448,14	
T_{solidus}	1745,86	981,6		2,96 10^2
T_{liquidus}	1793,15	1278,08		
T_{ref}	2273,15	1673,43	824,05	
T_{boil}	3133,15	2382,3		
T_{g}	3133,15	8472,3		6,09 10^3

The data above is shown in the next figure.

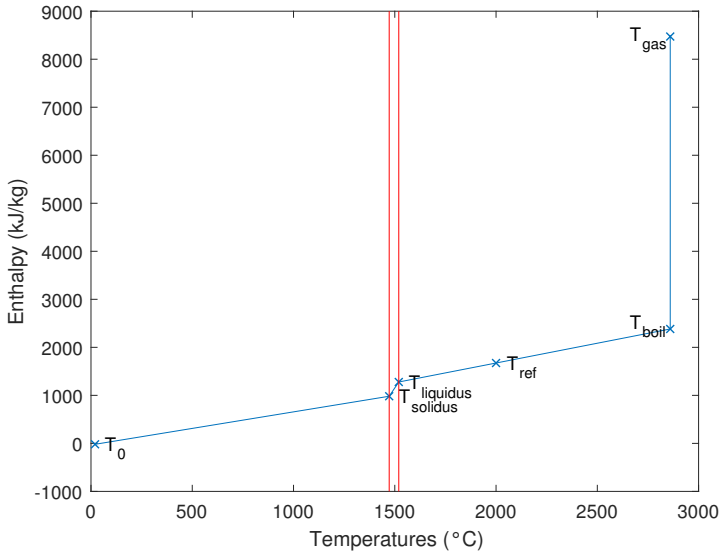

Figure C.5: Enthalpy and temperatures ER80S-G.

C.6. Pure Fe

Table C.6: Temperature, enthalpies and specific heat for pure Fe.

	Temperature K	Enthalpy kJ/kg	Specific heat (slope) J/kgK	Δi kJ/kg
T_0	293,15	-11,43	443,52	
T_{solidus}	1753,15	1003,88		2,79 10^2
T_{liquidus}	1803,15	1283,24	819,99	
T_{ref}	2273,15	1670,49	824,07	
T_{boil}	3133,15	2379,3		
T_{g}	3133,15	8469,3		6,09 10^3

The data above is shown in the next figure.

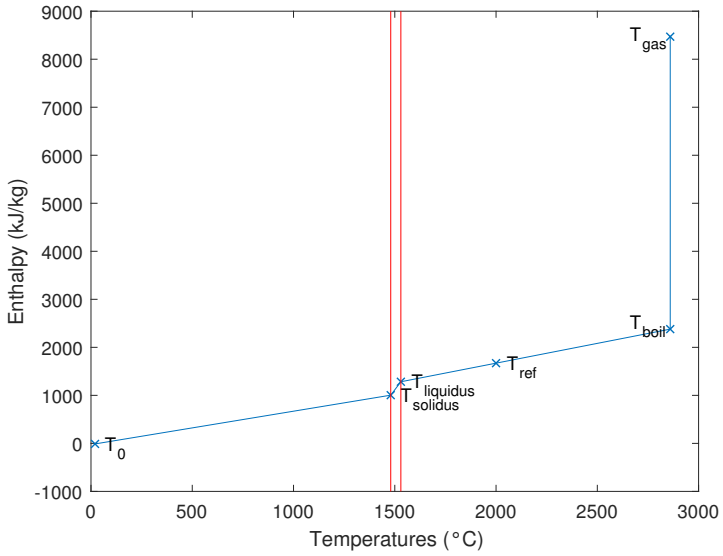

Figure C.6: Enthalpy and temperatures pure Fe.

C.7. ER70S-G

Table C.7: Temperature, enthalpies and specific heat for ER70S-G.

	Temperature K	Enthalpy kJ/kg	Specific heat (slope) J/kgK	Δi kJ/kg
T_0	293,15	-29,1	446,97	
T_{solidus}	1740,14	969,41		2,97 10^2
T_{liquidus}	1793,15	1265,96		
T_{ref}	2273,15	1662,49	826,43	
T_{boil}	3133,15	2373,4		
T_{g}	3133,15	8463,4		6,09 10^3

The data above is shown in the next figure.

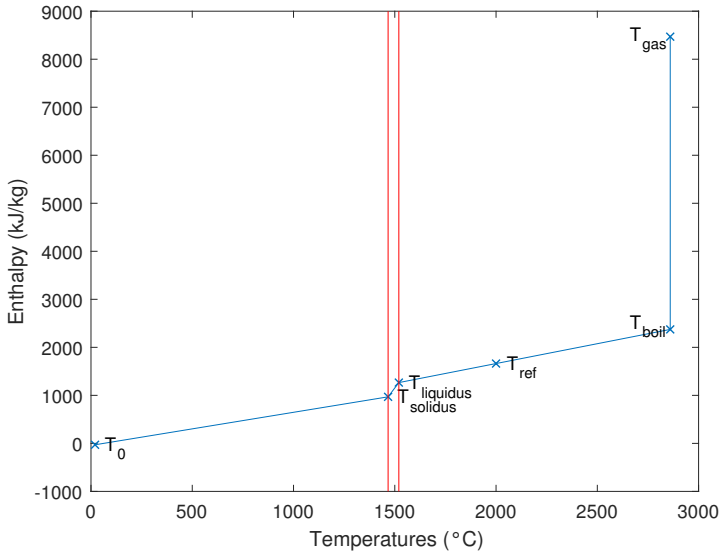

Figure C.7: Enthalpy and temperatures ER70S-G.

Appendant D

Notation

Variable	Unit	Description
q_{c}	W	cathode heat
q_{in}	J kg^{-1} s^{-1}	heat entering the control volume
q_{out}	J kg^{-1} s^{-1}	heat leaving the control volume
q_{gen}	J kg^{-1} s^{-1}	heat generated in the control volume
q_{st}	J kg^{-1} s^{-1}	heat stored in the control volume
q_{fall}	J kg^{-1} s^{-1}	heat generated by the fall of voltage
q_{arc}	J kg^{-1} s^{-1}	heat generated by the arc
q_{ct}	J kg^{-1} s^{-1}	heat generated by the contact tip
$q_{\mathrm{adv,in}}$	J kg^{-1} s^{-1}	heat entering by advection
V_{fall}	V	anode fall voltage
I	A	current of the process
$h_{\mathrm{arc,elec}}$	W m^{-2} K^{-1}	convection coefficient from the arc to droplet
A_{anode}	m^2	area of the anode spot
J_{a}	A m^{-2}	current density
k_{int}	W m^{-1} K^{-1}	thermal conductivity of argon
D_{d}	m	diameter of the droplet
ρ_{Ar}	kg m^{-3}	density argon
v_{Ar}	m s^{-1}	velocity of argon
μ_{Ar}	kg m^{-1} s^{-1}	dynamic viscosity argon
c_{p}^{Ar}	J kg^{-1} K^{-1}	specific heat argon
T_{ion}	K	temperature of ionization
R_{ct}	Ω	electrical resistance in the contact tip
L	m	length of the stick out (electrode extension)
ρ_{eff}	Ω m	effective electrical resistivity
A_{e}	m^2	effective area of the wire
U_{c}	m s^{-1}	Wire feed speed
$\dot{m}_{\mathrm{c}}$	kg s^{-1}	mass flow of the wire
m'_{c}	kg m^{-1}	linear mass flow
$\dot{m}_{\mathrm{d}}$	kg s^{-1}	Mass flow of droplet
$\dot{m}_{\mathrm{g}}$	kg s^{-1}	Mass flow evaporated

Variable	Unit	Description
i_0	J kg^{-1}	Enthalpy at room temperature
i_d	J kg^{-1}	Enthalpy of the droplet
i_g	J kg^{-1}	Enthalpy of the gas
Δi_ref	J kg^{-1}	Enthalpy change at T_{ref}
Δi_lg	J kg^{-1}	Enthalpy change liquidus-gas
T_d	K	Temperature droplet
$T_\mathrm{ref,s}$	K	Temperature reference solidus
$T_\mathrm{ref,l}$	K	Temperature reference liquidus
c_l	J kg^{-1} K^{-1}	Specific heat liquid
c_p	J kg^{-1} K^{-1}	Specific heat solid
H_C2^{+*}	-	normalized improved enthalpy
H_c	j kg^{-1}	enthalpy difference
ρ_0	Ω m	electrical resistivity at room temperature
ρ_m	Ω m	electrical resistivity at melting temperature
$\dot{m}_\mathrm{g}$"	kg s^{-1} m^{-2}	evaporation rate per area
A_d	m^2	area of the droplet
J	kg s^{-1} m^{-2} mol^{-1}	evaporation rate per area and mole
M	kg mol^{-1}	molar weight
d_c	m	diameter of the wire
γ	N m^{-1}	Surface tension
f	Hz	frequency of detachment
P_v	Pa	vapour pressure
R"$_\mathrm{tot}$	s m^{-1}	mass transfer resistance
R"$_\mathrm{surface}$	s m^{-1}	mass transfer resistance on surface
R"$_\mathrm{BL}$	s m^{-1}	mass transfer resistance on boundary layer
h_BL	m s^{-1}	resistance at boundary layer
D	m^2 s^{-1}	diffusivity
$\rho_\mathrm{max,T}$	kg m^{-3}	density at maximum temperature
h	m	arc length
M_Ar	kg mol^{-1}	molar mass argon
σ	A°	collision diameter
p	atm	ambient pressure
Re	-	Reynolds number
Pr	-	Prandtl number
Nu	-	Nusselt number
Sh	-	Sherwood number
Sc	-	Schmidt number
Acronyms		
WFS		Wire feed speed
CTWD		Contact tip to work distance